

# Intrinsic spin lifetime of conduction electrons in germanium

Pengke Li,<sup>1,\*†</sup> Yang Song,<sup>2,†</sup> and Hanan Dery<sup>1,2</sup>

<sup>1</sup>*Department of Electrical and Computer Engineering, University of Rochester, Rochester, New York 14627, USA*

<sup>2</sup>*Department of Physics and Astronomy, University of Rochester, Rochester, New York 14627, USA*

(Received 8 May 2012; published 2 August 2012)

We investigate the intrinsic spin relaxation of conduction electrons in germanium due to electron-phonon scattering. We derive intravalley and intervalley spin-flip matrix elements for a general spin orientation and quantify the resulting anisotropy in spin relaxation. The form of the intravalley spin-flip matrix element is derived from the eigenstates of a compact spin-dependent  $\mathbf{k}\cdot\mathbf{p}$  Hamiltonian in the vicinity of the  $L$  point (where thermal electrons are populated in Ge). Spin lifetimes from analytical integrations of the intravalley and intervalley matrix elements show excellent agreement with independent results from elaborate numerical methods.

DOI: [10.1103/PhysRevB.86.085202](https://doi.org/10.1103/PhysRevB.86.085202)

PACS number(s): 85.75.-d, 78.60.Fi, 71.70.Ej

## I. INTRODUCTION

Group IV semiconductors are natural material choices for quantum and classical spintronic devices.<sup>1-4</sup> Hyperfine interactions are suppressed due to the natural abundance of zero-spin nuclear isotopes. As a result, localized electrons have exceedingly long coherence times at low temperatures.<sup>5-7</sup> As for conduction electrons, space-inversion symmetry precludes their spin relaxation by the Dyakonov-Perel mechanism.<sup>8</sup> The intrinsic spin lifetime is therefore relatively long, reaching  $\sim 10$  ns at room temperature in nondegenerate  $n$ -type silicon.<sup>9-13</sup> Combined with the fact that silicon is the material of choice in the semiconductor industry, there is a wide interest in related spin injection experiments.<sup>14-18</sup>

The motivation for studying spin injection in Ge is similar to Si due to their shared properties and the compatibility with Si-based complementary metal-oxide semiconductor (CMOS) technology. Electrical spin injection and extraction in Ge have been recently investigated in lateral spin-transport devices with various doping profiles using nonlocal<sup>19</sup> and local<sup>20-26</sup> Hanle measurements, as well as in heterostructure and nanostructure devices.<sup>27,28</sup> Similar to direct band-gap semiconductors, optical orientation is an additional viable tool to investigate spin properties of electrons and holes in Ge.<sup>29-35</sup> Unlike silicon, optical orientation in Ge is efficient because of the energy proximity between the direct and indirect gaps. Spin-polarized electrons are first photoexcited to the  $\Gamma$  valley and then they relax via ultrafast spin conserving scattering to the conduction band edges in one of the four  $L$  valleys (located  $\sim 140$  meV below the zone center  $\Gamma$  valley).<sup>35</sup>

Theoretical efforts in the early days<sup>36,37</sup> were motivated by low-temperature electron spin resonance experiments that studied the  $g$  factor and spin-lattice relaxation of localized electrons in donor states.<sup>38-40</sup> On the other hand, little attention was paid to conduction electrons whose spin relaxation is mediated by the Elliott-Yafet mechanism.<sup>41,42</sup> By analyzing the space-inversion and time-reversal symmetries of the  $L$  point, Yafet deduced a  $T^{7/2}$  temperature dependence of the spin relaxation rate due to intravalley electron scattering with acoustic phonons.<sup>42</sup> Kalashnikov extended Yafet's theory to various statistical distributions and scattering mechanisms.<sup>43</sup> Chazalviel investigated spin flips due to electron-impurity scattering using effective spin-orbit coupling parameters that resemble the treatment in III-V semiconductors.<sup>44</sup> Most

recently, Tang *et al.* have used a tight-binding model to calculate the intrinsic spin relaxation of conduction electrons in Ge as a function of the energy split between the lowermost conduction valley and the other three valleys.<sup>12</sup> Such an energy split can be controlled by tuning the amplitude of a [111] uniaxial compressive strain.

In this paper we present a theory of spin-flip processes due to electron-phonon scattering in Ge. Two distinctive contributions are present in this work. First, we find the spin orientation dependence of spin-flip matrix elements. This dependence leads to anisotropy in spin relaxation and it is instrumental in analyzing measurements where the orientation of injected spins is set by the shape and magnetocrystalline anisotropy of ferromagnetic contacts or by the propagation and helicity of a circularly polarized light beam. An interesting result of the analysis is that most of the intrinsic spin relaxation of conduction electrons in Ge can be explained by coupling of the lowest conduction band to the upper conduction bands (rather than to the upper valence bands which is the typical case in most semiconductors). The second contribution of this work is the derivation of a spin-dependent  $\mathbf{k}\cdot\mathbf{p}$  Hamiltonian in the vicinity of the  $L$  point (conduction band edge). This compact Hamiltonian model exquisitely captures the signature of spin-orbit interaction on electronic states and it can be extended to study confined Ge structures using an expanded basis of envelope functions.<sup>45</sup>

This paper is organized as follows. Section II provides a theoretical framework for the electron-phonon interaction. Section III provides a quantitative discussion of intervalley spin flips due to scattering with zone-edge phonons. Using group theory, we derive the spin-flip matrix elements and find the resulting spin lifetime. Section IV deals with intravalley spin-flip processes and with the effects of spin-orbit coupling on low-energy conduction electrons. Using the method of invariants,<sup>46-49</sup> we derive a spin-dependent  $\mathbf{k}\cdot\mathbf{p}$  Hamiltonian around the  $L$  point. Eigenvectors of this Hamiltonian are then used to study intravalley spin flips due to scattering with long-wavelength acoustic phonons. Section V is a summary of findings and Appendices A–D contain technical details for interested readers.

## II. ELECTRON-PHONON INTERACTION

This section provides a theoretical framework for spin relaxation due to the interaction of electrons with the lattice ions.

It lays the foundation for the derived results in the following sections. We first express the electron-phonon scattering using the harmonic approximation,<sup>50,51</sup> and then write the resulting expression for the intrinsic spin relaxation rate. This section is concluded with the dependence of electronic states on spin orientation in crystals with a space-inversion center.

Consider an electron in a crystal with its quantum numbers  $\mathbf{k}_1$  and  $\mathbf{s}_1$  representing, respectively, the wave vector and spin state ( $\uparrow$  or  $\downarrow$ ). The band-index quantum number is omitted and unless otherwise noted we refer to states in the lowest conduction band. Following a scattering of this electron with a phonon, the transition amplitude into state  $\{\mathbf{k}_2, \mathbf{s}_2\}$  is given by<sup>13</sup>

$$\langle \mathbf{k}_2, \mathbf{s}_2; n_{\nu, \mathbf{q}} \pm 1 | \mathcal{H}_{\text{ep}}^{\nu}(\mathbf{q}) | \mathbf{k}_1, \mathbf{s}_1; n_{\nu, \mathbf{q}} \rangle = -\sqrt{\frac{\hbar^2}{2\varrho\Omega_{\nu, \mathbf{q}}V}} \sqrt{n_{\nu, \mathbf{q}} + \frac{1}{2} \pm \frac{1}{2}} \times M_{\nu}(\mathbf{k}_1, \mathbf{s}_1; \mathbf{k}_2, \mathbf{s}_2). \quad (1)$$

$n_{\nu, \mathbf{q}}$  is the phonon occupation (Bose-Einstein distribution at thermal equilibrium) where  $\nu$  is the phonon mode or symmetry (to become clear later) and  $\mathbf{q} = \mathbf{k}_2 - \mathbf{k}_1$  is the phonon wave vector. Phonon emission and absorption are described by the plus and minus signs, respectively. Other parameters are the phonon energy ( $\Omega_{\nu, \mathbf{q}}$ ), crystal mass density ( $\varrho$ ), and volume ( $V$ ). Finally, the matrix element reads

$$M_{\nu}(\mathbf{k}_1, \mathbf{s}_1; \mathbf{k}_2, \mathbf{s}_2) = \sum_{j, \alpha} \xi_{\alpha, \nu}(\mathbf{q}) e^{i\mathbf{q}\mathbf{R}_{j\alpha}} \cdot \langle \mathbf{k}_2, \mathbf{s}_2 | \nabla_r \mathcal{V}_{\text{at}}(\mathbf{r} - \mathbf{R}_{j\alpha}) | \mathbf{k}_1, \mathbf{s}_1 \rangle, \quad (2)$$

where  $j$  sums over the  $N$  primitive cells of the crystal and  $\alpha$  sums over atoms in a primitive cell. An atom position is then denoted by  $\mathbf{R}_{j\alpha}$ , its mode-dependent displacement vector by  $\xi_{\alpha, \nu}$ , and its potential including the spin-orbit coupling by

$$\mathcal{V}_{\text{at}}(\mathbf{r}) = V_{\text{at}}(\mathbf{r})\mathcal{I} + \frac{\hbar}{4m_0^2c^2} [\nabla V_{\text{at}}(\mathbf{r}) \times \mathbf{p}] \cdot \boldsymbol{\sigma}. \quad (3)$$

Spin-conserving scattering [ $\mathbf{s}_1 = \mathbf{s}_2$  in Eq. (2)] dominates the momentum relaxation where both spins are either up or down. Due to the small relativistic effect from spin-orbit coupling, spin-flip scattering ( $\mathbf{s}_1 = -\mathbf{s}_2$ ) is typically much weaker and leads to a relatively slow spin relaxation rate,<sup>13</sup>

$$\frac{1}{\tau_{s, \nu}} = \frac{2\pi\hbar}{\varrho N_c} \int d^3\mathbf{k}_1 \frac{\partial f(E_{\mathbf{k}_1})}{\partial E_{\mathbf{k}_1}} \int \frac{d^3\mathbf{k}_2}{(2\pi)^3} \frac{|M_{\nu}(\mathbf{k}_1, \mathbf{s}; \mathbf{k}_2, -\mathbf{s})|^2}{\Omega_{\nu}(\mathbf{q})} \times \sum_{\pm} \left( n_{\nu, \mathbf{q}} + \frac{1}{2} \pm \frac{1}{2} \right) \delta(E_{\mathbf{k}_2} - E_{\mathbf{k}_1} \pm \Omega_{\nu, \mathbf{q}}), \quad (4)$$

where  $f(E_{\mathbf{k}})$  is the statistical energy distribution of electronic states and  $N_c = \int d^3\mathbf{k} \partial f / \partial E_{\mathbf{k}}$  is an effective density of states constant. The weighted integration over  $\partial f / \partial E$  is exact at the limit of infinitesimal spin-dependent chemical potential splitting. It is valid for Fermi-Dirac statistics when the difference of chemical potentials between spin-up and spin-down populations is smaller than  $k_B T$ .

Evidently the determination of  $M_{\nu}(\mathbf{k}_1, \mathbf{s}; \mathbf{k}_2, -\mathbf{s})$  is the centerpiece in the theory of spin relaxation. For conduction electron transitions following a scattering by a phonon, the

initial and final states ( $|\mathbf{k}_1, \mathbf{s}_1\rangle$  and  $|\mathbf{k}_2, \mathbf{s}_2\rangle$ ) are located in conduction band valleys which are small pockets around some high symmetry points of the Brillouin zone. In intravalley and intervalley scattering, the initial and final states are located, respectively, in the same valley or in different valleys. The initial and final states can be expanded as linear combinations of eigenstates at their corresponding valley centers,

$$|\mathbf{k}, \mathbf{s}\rangle = \sum_{\ell} [a_{\ell}(\mathbf{k}) |\mathbf{K}_0, \ell, \uparrow\rangle + b_{\ell}(\mathbf{k}) |\mathbf{K}_0, \ell, \downarrow\rangle] e^{i\mathbf{k}' \cdot \mathbf{r}}, \quad (5)$$

where  $\mathbf{K}_0$  is the valley center point,  $\mathbf{k}' = \mathbf{k} - \mathbf{K}_0$ , and  $\ell$  sums over spin-independent energy bands. The coefficients,  $a_{\ell}(\mathbf{k})$  and  $b_{\ell}(\mathbf{k})$  are determined from the  $\mathbf{k} \cdot \mathbf{p}$  perturbation and also from the spin-orbit coupling perturbation term  $\lambda_{\text{so}} \nabla V(\mathbf{r}) \times (\mathbf{p} + \hbar\mathbf{k}') \cdot \boldsymbol{\sigma}$ , where  $V(\mathbf{r}) = \sum_{j, \alpha} V_{\text{at}}(\mathbf{r} - \mathbf{R}_{j\alpha})$  is the crystal potential and  $\lambda_{\text{so}} = \hbar/4m_0^2c^2$ . Mixed by spin-orbit interaction, the spin-up and spin-down states ( $\mathbf{s} = \{\uparrow, \downarrow\}$ ) are not the pure basis states of the spin subspace ( $\uparrow, \downarrow$ ).

In order to calculate the value of  $M_{\nu}(\mathbf{k}_1, \mathbf{s}; \mathbf{k}_2, -\mathbf{s})$ , we first decompose it into parts that belong to the irreducible representations (IRs) of the group at the wave vector  $\mathbf{K}_0$ , or at the wave vector connecting two valley centers for the case of intervalley scattering.<sup>52</sup> This decomposition of the matrix element involves parts that come from  $\mathbf{k} \cdot \mathbf{p}$  and spin-orbit coupling terms in the expansion of the initial and final states, as well as from  $\nabla_r \mathcal{V}_{\text{at}}(\mathbf{r} - \mathbf{R}_{j\alpha})$  in the electron-phonon interaction. Of course we can only determine by this procedure whether a particular integral is zero and what is the relation between two integrals if there is any. Nonetheless, this procedure allows us to recast the matrix element into a series of  $\mathbf{Q}$ -power terms where  $\mathbf{Q}$  represents the difference or average between  $\mathbf{k}_2 - \mathbf{K}_{0,2}$  and  $\mathbf{k}_1 - \mathbf{K}_{0,1}$ ,

$$M_{\nu}(\mathbf{k}_1, \mathbf{s}; \mathbf{k}_2, -\mathbf{s}) = D^{(0), \nu} + Q_i D_i^{(1), \nu} + Q_i Q_j D_{ij}^{(2), \nu} + \dots, \quad (6)$$

where summation over components (subscripts) of  $\mathbf{Q}$  is implied. The  $D^{(n), \nu}$  quantities, often called deformation potentials or scattering constants, are independent real constants resulting from the aforementioned selection rules (integral expressions of interactions between basis states). Values of these quantities are determined from explicit knowledge of the scattering potential and electronic states, and therefore numerical calculations or experimental input is needed.

The great advantage of the group theory approach is that it allows us to find a compact expression for the measurable spin relaxation rate. By substituting Eq. (6) into Eq. (4) one can readily identify the temperature dependence from the leading power of  $\mathbf{Q}$  (and from phonon population and dispersion). This procedure also allows one to identify the scattering angle dependence from the tensorial forms of  $D^{(n), \nu}$ . Furthermore, group theory can tell whether *intravalley* and/or *intervalley* are important in spin relaxation of a multivalley conduction band. It will be shown that intravalley spin flips in Ge are very weak since  $D^{(0)}$ ,  $D^{(1)}$ , and  $D^{(2)}$  in Eq. (6) vanish due to time reversal and space inversion symmetries. Intervalley scattering, on the other hand, will be shown as far more dominant in setting the

intrinsic spin relaxation rate, where in this case  $D^{(0)}$  does not vanish.

Finally, to account for possible anisotropy in spin relaxation, the analysis of both intravalley and intervalley spin flips should explicitly consider the dependence on spin orientation. In the case of centrosymmetric crystals (e.g., diamond structure of Ge), each band at wave vector  $\mathbf{k}$  is spin degenerate and we can define its states with respect to the spin orientation of the electron ( $\hat{s}$ ),<sup>42</sup>

$$\begin{aligned} \langle \mathbf{k}, \uparrow | \boldsymbol{\sigma} \cdot \hat{s} | \mathbf{k}, \uparrow \rangle &\equiv -\langle \mathbf{k}, \downarrow | \boldsymbol{\sigma} \cdot \hat{s} | \mathbf{k}, \downarrow \rangle \geq 0, \\ \langle \mathbf{k}, \uparrow | \boldsymbol{\sigma} \cdot \hat{s} | \mathbf{k}, \downarrow \rangle &\equiv 0, \end{aligned} \quad (7)$$

where  $\boldsymbol{\sigma}$  is a vector of Pauli matrices. Below we will find the explicit dependence of spin-flip matrix elements on the direction of  $\hat{s}$ .

### III. INTERVALLEY SPIN RELAXATION

Using group theory, we show in this section that intervalley spin-flip scattering in Ge is expressed in terms of two scattering constants. These constants are nonvanishing spin-flip matrix elements for electron scattering between different energy-minima points (valley centers):  $D_{\nu,s} = M_{\nu}(\mathbf{K}_{0,1}, \mathbf{s}; \mathbf{K}_{0,2}, -\mathbf{s})$ , where  $D_{\nu,s}$  bares the same meaning as the zeroth-order term in Eq. (6). In this case, we let  $\nu$  denote allowed phonon symmetries which, as explained later, include two types in bulk Ge. For scattering slightly away from the valleys centers, one can still assume  $M_{\nu}(\mathbf{k}_1, \mathbf{s}; \mathbf{k}_2, -\mathbf{s}) \simeq M_{\nu}(\mathbf{K}_{0,1}, \mathbf{s}; \mathbf{K}_{0,2}, -\mathbf{s})$  since in Ge and other multivalley semiconductors  $|\mathbf{K}_{0,1} - \mathbf{K}_{0,2}| \gg |\mathbf{k}_1 - \mathbf{K}_{0,1}|, |\mathbf{k}_2 - \mathbf{K}_{0,2}|$ . The spin-lifetime calculation is then substantially simplified since there is no need to rigorously calculate  $M_{\nu}(\mathbf{k}_1, \mathbf{s}; \mathbf{k}_2, -\mathbf{s})$  for each possible intervalley transition between states near the center points. Most importantly, since intervalley scattering is symmetry allowed in the lowest order (i.e., nonzero between different  $L$  points), group theory alone is sufficient to find the exact form of the spin-flip matrix elements *together with their dependence on spin orientation*.

Figure 1(a) shows a scheme of the four conduction-band valleys in Ge where the vertical arrow marked by  $\mathbf{q}_{001}$  represents one possible intervalley scattering between different valleys. Thermal electrons in unstrained bulk Ge are located

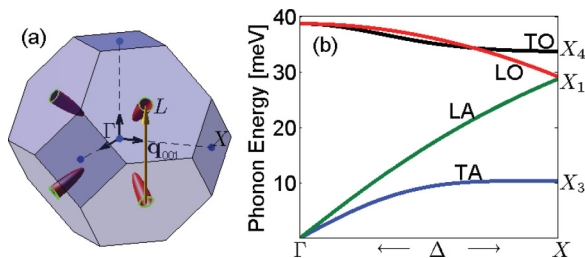


FIG. 1. (Color online) (a) The four conduction-band valleys of Ge. Centers of their ellipsoidal energy surfaces are located at the zone-edge  $L$  points (energy minima). The vertical  $\mathbf{q}_{001}$  arrow represents one of six equivalent intervalley transitions between valley centers. (b) Phonon dispersion along the  $\Gamma$ - $\Delta$ - $X$  symmetry axis [dashed lines in (a)] and symmetry notations of zone-edge  $X$  phonon modes. Electrons are transferred between different valleys [e.g., the  $\mathbf{q}_{001}$  arrow in (a)] by emission or absorption of phonons near the  $X$  point.

in these four valleys whose centers are the  $L$  points in the edge of the Brillouin zone. The crystal momentum difference between valley centers can be mediated by  $X$  point phonons. For example, the  $L_{111}$  and  $L_{1\bar{1}\bar{1}}$  centers [ $\mathbf{k} = \pi/a(1, 1, \pm 1)$ ] are connected by  $X_{001}$  [ $\mathbf{q}_{001} = 2\pi/a(0, 0, 1)$ ]. Figure 1(b) shows the symmetry notations of these zone-edge phonons along with their dispersion along the  $\Gamma$ - $\Delta$ - $X$  symmetry axis. These results are calculated from an adiabatic bond-charge model of bulk Ge.<sup>53</sup> The zone-edge phonons belong to three two-dimensional (2D) irreducible representations:  $X_3$  (TA, 10 meV),  $X_1$  (LA and LO, 29 meV), and  $X_4$  (TO, 33 meV),<sup>54</sup> with their modes and energies written in parentheses.

Group theory is used to derive selection rules for intervalley scattering. These selection rules are derived from common symmetry operations of the little groups at two valley centers  $\mathbf{K}_{0,1}$ ,  $-\mathbf{K}_{0,2}$  and their difference  $\mathbf{K}_{0,1} - \mathbf{K}_{0,2}$ . Technical details of applying this approach in Ge are given in Appendix A and here we summarize the main findings. Excluding the spin degree of freedom, the selection rule for transition between valleys that we denote by  $L$  and  $L_t$  reads  $L_1 \otimes L_{1t} = X_1 \oplus X_3$ , where  $L_1$  is the irreducible representation (IR) of electron states in the minima of the conduction band. Intervalley scattering with phonons of  $X_3$  symmetry is forbidden by time-reversal symmetry and not by the space-group symmetry.<sup>55,56</sup> This rule means that a single constant  $D_{\nu=X_1,m}$  is needed to describe spin-independent intervalley scattering (momentum relaxation). Including the spin degree of freedom, it is convenient to use double group theory where  $L_1$  is replaced by  $L_6$  and the new selection rule reads<sup>12</sup>

$$L_6 \otimes L_{6t} = 2X_1 \oplus X_4 \oplus X_3. \quad (8)$$

This rule means that three independent scattering parameters are needed to fully describe spin-conserving and spin-flip intervalley scattering (two are related to the  $X_1$  symmetry and one to  $X_4$ ). This selection rule does not provide information on the spin orientation dependence which is most important in analyzing experiments. To overcome this shortcoming, we can work with IR matrices rather than their traces.<sup>13</sup> Technical details are given in Appendix A and here we provide the final result. The spin orientation  $\hat{s}$  is described by a polar angle ( $\theta$ ) from the  $+z$  crystallographic axis and an azimuthal angle ( $\phi$ ) in the  $xy$  plane measured from the  $+x$  direction. For a spin-flip transition between  $L_{111}$  and  $L_{1\bar{1}\bar{1}}$  points (via a zone-edge phonon with wave vector  $\mathbf{q}_{001}$ ), the square amplitude of the matrix element reads

$$\begin{aligned} &|M_{\nu}(\mathbf{k}_{L_{111}}, \mathbf{s}; \mathbf{k}_{L_{1\bar{1}\bar{1}}}, -\mathbf{s})|^2 \\ &= \begin{cases} 2D_{X_1,s}^2 (1 + \cos^2 \theta + \sin 2\phi \sin^2 \theta) & \text{if } \nu = X_1 \\ 2D_{X_4,s}^2 \sin^2 \theta & \text{if } \nu = X_4 \end{cases}. \end{aligned} \quad (9)$$

Both phonon symmetries share a prefactor of 2 due to the twofold degeneracy in the  $X$  point of a diamond crystal structure. For the remaining five transitions between other combinations of  $L$  points, Eq. (9) varies according to a straightforward coordinate transformation. These results are summarized in Table I [also see discussion of Eq. (A24) in Appendix A]. As seen by the right column of the table, spin flips due to scattering with  $X_4$  phonons vanish if the spin is oriented parallel to the phonon wave vector [ $z$  axis for the case of  $\mathbf{q}_{001}$  in Eq. (9); i.e.,  $\theta = 0$ ]. If the spin

TABLE I.  $|M_{X_i}(\mathbf{k}_L, \mathbf{s}; \mathbf{k}_{L_i}, -\mathbf{s})|^2/2D_{X_i}^2$  for intervalley spin-flip transitions of all six valley-to-valley configurations.

$L \leftrightarrow L_i$	$X_1$	$X_4$
$L_{111} \leftrightarrow L_{11\bar{1}}$	$1 + \cos^2 \theta + \sin^2 \theta \sin 2\phi$	$1 - \cos^2 \theta$
$L_{111} \leftrightarrow L_{1\bar{1}\bar{1}}$	$1 + \sin^2 \theta \sin^2 \phi + \sin 2\theta \cos \phi$	$1 - \sin^2 \theta \sin^2 \phi$
$L_{111} \leftrightarrow L_{\bar{1}\bar{1}\bar{1}}$	$1 + \sin^2 \theta \cos^2 \phi + \sin 2\theta \sin \phi$	$1 - \sin^2 \theta \cos^2 \phi$
$L_{\bar{1}\bar{1}\bar{1}} \leftrightarrow L_{11\bar{1}}$	$1 + \sin^2 \theta \sin^2 \phi - \sin 2\theta \cos \phi$	$1 - \sin^2 \theta \sin^2 \phi$
$L_{\bar{1}\bar{1}\bar{1}} \leftrightarrow L_{1\bar{1}\bar{1}}$	$1 + \cos^2 \theta - \sin^2 \theta \sin 2\phi$	$1 - \cos^2 \theta$
$L_{1\bar{1}\bar{1}} \leftrightarrow L_{11\bar{1}}$	$1 + \sin^2 \theta \cos^2 \phi - \sin 2\theta \sin \phi$	$1 - \sin^2 \theta \cos^2 \phi$

orientation and phonon wave vector are perpendicular, the  $X_4$  spin flips are described by a single independent nonvanishing matrix-element constant  $D_{v=X_4,s}$ . For the  $X_1$  phonons, one of the two independent nonvanishing matrix elements in Eq. (8) is attributed to spin-flip scattering ( $D_{v=X_1,s}$ ) and the other to spin-conserving scattering ( $D_{v=X_1,m}$ ). Values of these scattering constants can be extracted from experiments or from rigorous numerical calculations as discussed in Appendix B where we find  $D_{X_1,s} = 35 \text{ meV/\AA}$  and  $D_{X_4,s} = 46 \text{ meV/\AA}$ . As will be shown, these comparable constants set the spin relaxation rate. It is understood that the much larger spin-conserving scattering constant  $D_{v=X_1,m}$  is irrelevant to the analysis of spin relaxation (independent of the spin-orbit coupling).

Having the spin-flip matrix elements in Table I, we calculate the intervalley spin relaxation rate [Eq. (4)] for a Boltzmann distribution of electrons,

$$\frac{1}{\tau_{s,\text{inter}}} = \frac{4}{3} \left( \frac{2m_d}{\pi} \right)^{\frac{3}{2}} \sum_{i=1,4} \frac{A_i(\theta, \phi) D_{X_i,s}^2}{\hbar^2 \rho \sqrt{\Omega_i}} \frac{\vartheta(y_i)}{\exp(y_i) - 1}. \quad (10)$$

$\rho = 5.323 \text{ g/cm}^3$  is the crystal density and  $m_d = 0.22m_0$  is the effective electron mass in bulk Ge.<sup>57</sup>  $\vartheta(y_i = \Omega_i/k_B T) = \sqrt{y_i} \exp(y_i/2) K_{-1}(y_i/2)$  is associated with the modified Bessel function of the second kind. For both phonon energies ( $\Omega_1 = 29 \text{ meV}$  and  $\Omega_4 = 33 \text{ meV}$ ), this term slightly depends on temperature in the range between 10 and 400 K such that  $2 < \vartheta(\Omega_i/k_B T) < 4$ . On the other hand, most of the temperature dependence of the intervalley relaxation rate comes from the thermal population of zone-edge phonons [exponent term in the denominator of Eq. (10)]. This population is strongly suppressed at low temperatures. Finally, the scattering constants  $D_{X_1,s} = 35 \text{ meV/\AA}$  and  $D_{X_4,s} = 46 \text{ meV/\AA}$  are, respectively, weighted by  $A_1(\theta, \phi)$  and  $A_4(\theta, \phi)$  that include the dependence on spin orientation (Table I). We discuss their explicit angular dependence for several general cases.

*No strain or [100] strain:* The four  $L$  valleys in the lowest conduction band are degenerate and transitions between all six pairs of valleys are equivalent. The anisotropy in spin relaxation due to intervalley scattering between two valleys is compensated by opposite anisotropy of other pairs. The sum of expressions in each of the two columns of Table I is independent of  $\theta$  and  $\phi$ ,

$$A_1 = 8, \quad A_4 = 4. \quad (11)$$

As shown next, when the symmetry between different valleys is broken, the dependence of the intervalley matrix elements on spin orientation lends itself to a measurable anisotropy in the spin lifetime.

*[111] strain:* The case of uniaxial compressive strain results in a single low-energy valley (along the strain axis) and three higher energy valleys. At relatively large strain levels ( $\sim 1\%$ ), the energy split is large enough to quench the intervalley spin relaxation mechanism.<sup>12</sup> This effect amounts to assigning  $1/\tau_{s,\text{inter}} = 0$ . On the other hand, in biaxial compressive strain configuration (or uniaxial tensile strain) three of the valleys shift down in energy and one valley shifts up. Excluding transitions with the  $L_{111}$  valley (considering the last three lines in Table I) we get

$$A_1 = \frac{16 - 4 \sin^2 \theta \sin 2\phi - 4 \sin 2\theta (\cos \phi + \sin \phi)}{3},$$

$$A_4 = \frac{8}{3}. \quad (12)$$

This strain configuration restores the anisotropy in spin relaxation due to electron scattering with  $X_1$  zone-edge phonons. By changing the spin orientation from the [111] strain axis to its perpendicular plane,  $\tau_{s,\text{inter}}$  drops by  $\sim 50\%$  [changing  $A_1$  from  $8/3$  to  $20/3$  in Eq. (10)].

*[110] strain:* This strain configuration is optimal for detection of the anisotropy since intervalley transitions are effective from a single pair of valleys. Consider, for example, the case that  $L_{111}$  and  $L_{11\bar{1}}$  valleys shift sufficiently down in their energy. Then, only the first term in Table I represents the intervalley scattering and we get

$$A_1 = 2(1 + \cos^2 \theta + \sin 2\phi \sin^2 \theta), \quad A_4 = 2 \sin^2 \theta. \quad (13)$$

The anisotropy in spin relaxation is now caused by electron scattering with both types of zone-edge phonons. By changing the spin orientation from the strain axis to its perpendicular plane,  $\tau_{s,\text{inter}}$  [Eq. (10)] is doubled.

Other than strain, it should also be possible to observe the anisotropy by applying electric fields of a few kV/cm along the mentioned directions. Here, valley repopulation will result in preferential scattering from hot-to-cold valleys.<sup>58</sup> Finally, by averaging over spin orientations in Eqs. (12) and (13), the spin lifetime [Eq. (10)] with two (three) low-energy valleys is about 3 (3/2) times longer than that of the unstrained case. The reason is that electrons can scatter to one (two) valleys rather than three.

The solid curve in Fig. 2 shows the temperature dependence of the intervalley spin lifetime in unstrained bulk Ge [Eq. (10) with  $A_1 = 8$  and  $A_4 = 4$ ]. We have also performed rigorous numerical integrations of Eq. (4) in which  $M_v(\mathbf{k}_1, \mathbf{s}; \mathbf{k}_2, -\mathbf{s})$  rather than  $M_v(\mathbf{k}_{L_{111}}, \mathbf{s}; \mathbf{k}_{L_{11\bar{1}}}, -\mathbf{s})$  is evaluated in the integration. The calculation of the matrix element follows the analysis in Appendix B. Whereas this numerical approach is not transparent compared with the group theory analysis, it takes into account higher-order corrections due to the slight variation of the matrix element when departing from the center of the valleys. Nonetheless, the complete numerical results for scattering with all  $X$  point phonons [red pentagram markers in Fig. 2] show that the zeroth-order analytical calculation is an excellent approximation [Eq. (10)]. The black diamond markers denote numerical results due to scattering with  $X_3$  phonons. Their zeroth-order contribution vanishes by time-reversal symmetry [Eq. (8)], while their first-order contribution is allowed [ $D^{(1),v=X_3}$  is the lowest-order nonvanishing term in Eq. (6)]. In spite of their vanishing contribution at the

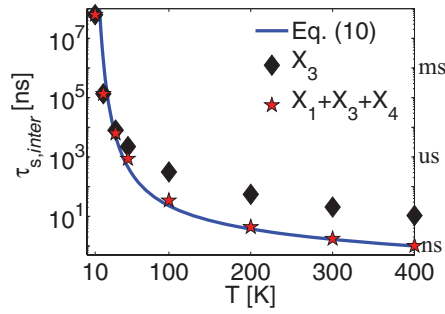


FIG. 2. (Color online) Calculated temperature dependence of the intrinsic spin lifetime in unstrained Ge due to intervalley scattering of electrons. The solid line follows Eq. (10) with  $A_1 = 8$  and  $A_4 = 4$ . At room temperature, the resulting spin lifetime is  $\sim 1$  ns. The markers are from rigorous numerical results (see text). Black diamonds denote contributions from  $X_3$  phonons and red pentagrams from all  $X$  point phonon symmetries.

lowest order, Fig. 2 shows that  $X_3$  phonons have non-negligible contribution in low temperatures. This property can be understood by the relatively large population of  $X_3$  phonons compared with that of  $X_1$  and  $X_4$  phonons [ $n_{v,q}$  in Eq. (4)]. At low temperatures, the zone-edge phonon population reads  $\exp(-\Omega_i/k_B T)$ , and therefore it is much larger in the case of  $X_3$  phonons [ $\Omega_3 \sim 10$  meV and  $\Omega_{1,4} \sim 30$  meV; see Fig. 1(b)].

#### IV. $L$ -POINT HAMILTONIAN AND INTRAVALLEY SPIN RELAXATION

Intravalley spin-flip matrix elements in Ge are much smaller than in the intervalley case. This weak effect of intravalley processes stems from space-inversion and time-reversal symmetries of the low-energy conduction states in Ge.<sup>42</sup> The intravalley process becomes important, however, when quenching the intervalley process by applying strain or strong electric fields such that the electrons are located in a single conduction valley. Tang *et al.* have shown that the spin lifetime is then increased from 1 ns to the range of 100 ns.<sup>12</sup> In this work we quantify the strong anisotropy of the intravalley spin relaxation in Ge and show that when orienting the spin along the [111] crystal axis the intravalley spin lifetime is further suppressed and reaches the scale of 1  $\mu$ s in room temperature. In addition, we derive a spin-dependent  $\mathbf{k}\cdot\mathbf{p}$  Hamiltonian in the vicinity of the  $L$  point and correlate its parameters with spin relaxation processes.

To gain better understanding of the intravalley spin flips in Ge, we break this section into three parts, where each part relies on its former. First we discuss general symmetry properties of conduction electrons in Ge with an emphasis on the effect of spin-orbit coupling. In the second part we make use of these findings to derive a compact Hamiltonian matrix using a relatively small set of  $L$ -point basis functions. We keep technical aspects of this derivation to Appendix C. Using the spin-dependent eigenvectors of the derived Hamiltonian, we introduce the concept of overlap integrals. This information combined with deformation potential theory is then used in the last part of this section to derive the intravalley spin-flip matrix elements, the resulting spin lifetime, and the dependence on

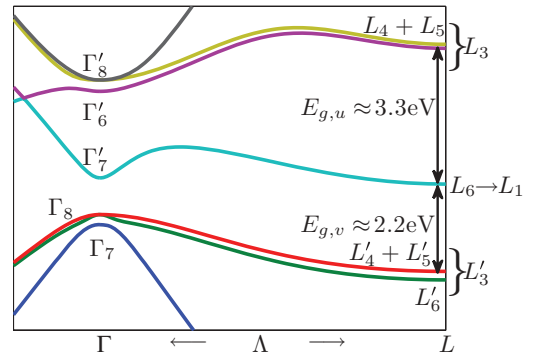


FIG. 3. (Color online) Calculated band structure of Ge along the  $\Gamma$ - $\Lambda$ - $L$  symmetry axis following the results of an empirical pseudopotential method.<sup>59</sup> Appendix B includes technical numerical details of this calculation. The conduction-band edge is indicated by the irreducible representation  $L_1$  ( $L_6$ ) in single (double) group notation.<sup>60,61</sup>

spin orientation. Appendix D includes technical information on the difference between intravalley spin flips in Si and Ge.

#### A. Symmetry effects on electronic states in Ge

Figure 3 shows the energy band structure of unstrained bulk Ge along the  $\Gamma$ - $\Lambda$ - $L$  symmetry axis. The conduction edge is indicated by  $L_1$ , where thermal conduction electrons can reside in four equivalent conduction valley minima [Fig. 1(a)]. Using the  $L$ -point symmetry notations in Fig. 3, we explain the symmetries of wave functions in the vicinity of this point.

Representations of conduction (valence) states in the  $L$  point have even (odd) parity under space-inversion operation. In the notation of single group theory, there are six irreducible representations (IR) of the  $L$ -point space group.<sup>60,61</sup> The lowest conduction band is nondegenerate and belongs to  $L_1$  (a one-dimensional IR). Figure 3 shows that nearby bands are pairs of valence and conduction bands. They are represented, respectively, by the two-dimensional IRs  $L'_3$  and  $L_3$ . If the crystal potential is vanishingly small then the  $L$ -point energies of these five bands ( $L_1$ ,  $L_3$ , and  $L'_3$ ) are degenerate. However, the crystal potential in Ge splits these bands into three sets and the relatively large energy separation from  $L_1$  will be shown to result in a very slow intravalley spin relaxation process. In comparison, the six conduction band valleys in Si are located close (in energy and wave vector) to the two-band degeneracy in the  $X$  point. This degeneracy leads to a spin hot spot along certain directions in the square boundary faces of the Brillouin zone,<sup>9,10,13</sup> and to a unique behavior of intravalley spin relaxation in Si.<sup>13</sup> This distinct difference between Si and Ge merits independent treatments of the spin relaxation.

The wave functions of conduction electrons  $|\mathbf{k}, \uparrow(\downarrow)\rangle$  include small contributions from states of remote bands. In the  $\mathbf{k}\cdot\mathbf{p}$  theory there are two first-order terms related to signatures of the spin-orbit interaction,

$$H_{so} = \frac{\hbar}{4m_0^2 c^2} \nabla V \times \mathbf{p} \cdot \hat{\sigma}, \quad (14)$$

$$H_{so}^k = \frac{\hbar^2}{4m_0^2 c^2} \nabla V \times \mathbf{k} \cdot \hat{\sigma}, \quad (15)$$

where throughout this section the value of  $\mathbf{k}$  is measured from its nearby valley center ( $L$  point).  $H_{\text{so}}^k$  transforms as a polar vector ( $\nabla V$ ) and can couple between odd and even states. In our case, the coupling is between states of  $L_1$  and  $L'_3$  symmetries that represent, respectively, the lowest conduction band and upper valence bands. On the other hand,  $H_{\text{so}}$  transforms as an axial vector ( $\nabla V \times \mathbf{p}$ ) and can couple the even states of  $L_1$  and  $L_3$  (lowest and upper conduction bands). The dimensionality of  $L'_3$  or  $L_3$  (2D IRs) is such that each is coupled to  $L_1$  by two components of a vector that lie perpendicular to the valley axis [i.e., parallel to the hexagonal boundary faces at the zone edge; see Fig. 1(a)].

### B. $L$ -point Hamiltonian

In this part we expand the wave functions of electrons using the  $L$ -point basis states. The expansion allows us to identify important signatures of spin-orbit coupling on the wave functions and then to correlate them with spin relaxation processes. Near the valley center, the wave function is approximated by

$$|\mathbf{k}, \mathbf{s}\rangle = \left[ \sum_{\gamma=1,3,3'} C_{\gamma}(\mathbf{k}, \mathbf{s}) |L_{\gamma}\rangle \right] e^{i(\mathbf{k}_L + \mathbf{k}) \cdot \mathbf{r}}. \quad (16)$$

Using the relation between spin-up and spin-down states [Eq. (7)], and following the previous discussion on  $L_1$ ,  $L_3$ , and  $L'_3$  states, we write

$$\begin{aligned} C_{\gamma}(\mathbf{k}, \uparrow) |L_{\gamma}\rangle &= \sum_{m=1}^{N_{\gamma}} a_{m,\gamma}(\mathbf{k}) |L_{\gamma}^m, \uparrow\rangle + b_{m,\gamma}(\mathbf{k}) |L_{\gamma}^m, \downarrow\rangle, \\ C_{\gamma}(\mathbf{k}, \downarrow) |L_{\gamma}\rangle &= \sum_{m=1}^{N_{\gamma}} a_{m,\gamma}^*(\mathbf{k}) |L_{\gamma}^m, \downarrow\rangle - b_{m,\gamma}^*(\mathbf{k}) |L_{\gamma}^m, \uparrow\rangle. \end{aligned} \quad (17)$$

Totally we consider ten spin-dependent basis states: Two from the nondegenerate lowest conduction band ( $N_1 = 1$ ), and four from either the upper conduction or valence bands (each being two-band degenerate in the absence of spin-orbit coupling,  $N_3 = N_{3'} = 2$ ). The coefficients are eigenvectors of the  $10 \times 10$  Hamiltonian matrix,

$$\begin{pmatrix} H_{33} + E_{g,u} & H_{13}^{\dagger} & H_{33'} \\ H_{13} & H_{11} & H_{13'} \\ H_{33'} & H_{13'}^{\dagger} & H_{33'} - E_{g,v} \end{pmatrix} \begin{pmatrix} C_3 \\ C_1 \\ C_3' \end{pmatrix} = E \begin{pmatrix} C_3 \\ C_1 \\ C_3' \end{pmatrix}, \quad (18)$$

where  $H_{ij}$  is a matrix block denoting the spin and wave vector dependent coupling between basis states with  $L_i$  and  $L_j$  symmetries.  $E_{g,u}$  and  $E_{g,v}$  denote, respectively, the  $L$ -point energy separations of the lowest conduction band from the upper conduction and upper valence bands (see Fig. 3). Below we present the Hamiltonian matrix using the basis functions of the  $L_{111}$  point [ $\mathbf{k}_L = \pi(1,1,1)/a$ ]. Matrix forms in the  $\langle \bar{1}11 \rangle$ ,  $\langle 1\bar{1}1 \rangle$ , and  $\langle 11\bar{1} \rangle$  valleys are derived by trivial coordinate transformation. In addition, to derive a compact matrix form we use a rotated set of Cartesian coordinates,

$$\hat{\mathbf{w}} = \frac{\hat{\mathbf{x}} - \hat{\mathbf{y}}}{\sqrt{2}}, \quad \hat{\mathbf{u}} = \frac{\hat{\mathbf{x}} + \hat{\mathbf{y}} - 2\hat{\mathbf{z}}}{\sqrt{6}}, \quad \hat{\mathbf{\lambda}} = \frac{\hat{\mathbf{x}} + \hat{\mathbf{y}} + \hat{\mathbf{z}}}{\sqrt{3}}. \quad (19)$$

$\hat{\mathbf{u}}$  and  $\hat{\mathbf{w}}$  lie parallel to the hexagonal boundary face [Fig. 1(a)].  $\hat{\mathbf{\lambda}}$  is along the valley axis connecting the  $\Gamma$  and  $L_{111}$  points.

We construct the Hamiltonian matrix [Eq. (18)] using the method of invariants.<sup>46–49</sup> Application of this method with relevance to the  $L$  point is given in Appendix C. Here we summarize the findings. The lowest conduction band is associated with the identity IR and contributes a trivial  $2 \times 2$  matrix form ( $L_1 \otimes L_1 = L_1$ ),

$$H_{11} = \left[ \frac{\hbar^2(k_u^2 + k_w^2)}{2m_t^*} + \frac{\hbar^2 k_{\lambda}^2}{2m_l^*} \right] \otimes I_{2 \times 2}. \quad (20)$$

$m_t^*$  and  $m_l^*$  are effective mass parameters representing the effect of remote bands (outside the chosen basis states). Matrix blocks of the upper valence bands or upper conduction bands share a similar form ( $L_3 \otimes L_3 = L'_3 \otimes L'_3 = L_1 + L_2 + L_3$ ),

$$H_{ii} = \left[ \frac{\hbar^2(k_u^2 + k_w^2)}{2m_{t,i}^*} + \frac{\hbar^2 k_{\lambda}^2}{2m_{l,i}^*} \right] \otimes I_{4 \times 4} + \Delta_i \rho_y \otimes \sigma_{\lambda}, \quad (21)$$

where  $i = 3$  or  $i = 3'$ . The mass parameters have similar meaning as in  $H_{11}$ .  $\Delta_i$  denotes the internal spin-orbit coupling between the two  $L_i$  basis functions.  $\rho_y = \sigma_y$  originates from the two-band degeneracy in the absence of spin-orbit coupling.

The off-diagonal matrix block  $H_{13'}$  denotes the coupling between the lowest conduction band and upper valence bands. Its form follows from  $L_1 \otimes L'_3 = L'_3$ ,

$$H_{13'} = P(k_w[0,1] - k_u[1,0]) \otimes I_{2 \times 2} + i\alpha[(\mathbf{k} \times \boldsymbol{\sigma})_w \otimes [0,1] - (\mathbf{k} \times \boldsymbol{\sigma})_u \otimes [1,0]], \quad (22)$$

where  $[1,0]$  and  $[0,1]$  are ordinary  $1 \times 2$  matrices. Their Kronecker products with  $2 \times 2$  matrices indicate that  $H_{13'}$  is a  $2 \times 4$  matrix.  $P$  and  $\alpha$  are two independent matrix element constants that originate from the  $\mathbf{k} \cdot \mathbf{p}$  and  $H_{\text{so}}^k$  perturbation terms, respectively. The coupling matrix of the lowest and upper conduction bands is wave vector independent and it follows from  $L_1 \otimes L_3 = L_3$ :

$$H_{13} = i\Delta_L(\sigma_u \otimes [1,0] + \sigma_w \otimes [0,1]) \otimes I_{2 \times 2}, \quad (23)$$

where  $\Delta_L$  denotes the direct spin-orbit coupling between these bands. Finally, the  $4 \times 4$  coupling matrix between the upper valence and conduction bands follows from  $L'_3 \otimes L_3 = L'_1 + L'_2 + L'_3$ :

$$H_{33'} = [P_1(ik_u\rho_y - k_w I_{2 \times 2}) + P_2 k_{\lambda} \rho_x] \otimes I_{2 \times 2}, \quad (24)$$

where we have neglected the  $H_{\text{so}}^k$  coupling between these bands since it plays a negligible role in the spin relaxation of conduction-valley electrons. Table V in Appendix C lists the values of all parameters in Eqs. (20)–(24). This Appendix also includes a discussion of the empirical pseudopotential method used to derive these parameter values.

Given the relatively large  $L$ -point energy gaps, the energy dispersion of electrons in  $L$  valleys is well approximated by eigenvalues of the reduced  $2 \times 2$  matrix:  $H_{11} + H_{13'} H_{13'}^{\dagger} / E_{g,v} - H_{13} H_{13}^{\dagger} / E_{g,u}$ ,

$$E_c = \frac{2\Delta_L^2}{E_{g,u}} + \frac{\hbar^2(k_u^2 + k_w^2)}{2m_t} + \frac{\hbar^2 k_{\lambda}^2}{2m_l}. \quad (25)$$

The constant energy shift is due to the direct spin-orbit coupling with the upper conduction bands. The effective mass

parameters are

$$\frac{1}{m_t} = \frac{1}{m_t^*} + \frac{2P^2 + 2\alpha^2}{\hbar^2 E_{g,v}}, \quad \frac{1}{m_l} = \frac{1}{m_l^*} + \frac{4\alpha^2}{\hbar^2 E_{g,v}}.$$

About half of the anisotropy between the transverse and longitudinal effective masses in Ge ( $m_t \approx 0.08m_0$  and  $m_l \approx 1.6m_0$ ) is set by the spin independent coupling with the upper valence bands ( $P = 9 \text{ eV \AA}$ ).<sup>57</sup> The spin-orbit coupling signatures on the energy dispersion are negligible and can be ignored ( $\alpha = 40 \text{ meV \AA}$  and  $\Delta_L = 27 \text{ meV}$ ). On the other hand, the minute effect of spin-orbit coupling on the eigenvectors of Eq. (18) sets the time scale for spin relaxation. Choosing the spin quantization along the valley axis, the spin-up eigenvector along this direction [ $\hat{s} = \hat{\lambda}$  in Eq. (7)] reads

$$\begin{aligned} \mathbf{C}_1(\mathbf{k}, \uparrow_\lambda) &= [1, g(\mathbf{k})] + O(k^2), \\ \mathbf{C}_3(\mathbf{k}, \uparrow_\lambda) &= \frac{\Delta_L}{E_{g,u}} [0, -1, 0, i] + O(k^2), \\ \mathbf{C}'_3(\mathbf{k}, \uparrow_\lambda) &= \frac{P}{E_{g,v}} [-k_u - i\gamma_3 k_w, f_+(\mathbf{k}), \\ &\quad k_w - i\gamma_3 k_u, f_-(\mathbf{k})] + O(k^3). \end{aligned} \quad (26)$$

The components of the spin-down eigenvector [ $\mathbf{C}_i(\mathbf{k}, \downarrow_\lambda)$ ] are readily obtained from space-inversion and time-reversal relations [Eq. (17)]. The  $g(\mathbf{k})$  and  $f_\pm(\mathbf{k})$  functions in  $\mathbf{C}_1$  and  $\mathbf{C}'_3$  read

$$\begin{aligned} g(\mathbf{k}) &= \frac{P^2}{E_{g,v}^2} [k_u f_+(\mathbf{k}) - k_w f_-(\mathbf{k})], \\ f_\pm(\mathbf{k}) &= r_\pm [\gamma_1 (k_w - i k_u) \pm i \gamma_2 k_\lambda], \end{aligned} \quad (27)$$

where  $r_+ = 1$  and  $r_- = -i$ . The  $\gamma_j \ll 1$  parameters scale with three of the spin-orbit coupling constants ( $\alpha$ ,  $\Delta_3$ , and  $\Delta_L$ ) whose values are given in Table V,

$$\gamma_1 = \frac{\Delta_L}{E_{g,u}} \frac{P_1}{P} \approx 0.006, \quad (28a)$$

$$\gamma_2 = \frac{\alpha}{P} + \frac{\Delta_L}{E_{g,u}} \frac{P_2}{P} \approx 0.005, \quad (28b)$$

$$\gamma_3 = \frac{\alpha}{P} + \frac{\Delta_3}{E_{g,v}} \approx 0.05. \quad (28c)$$

The internal spin-orbit coupling in the valence band ( $\Delta_3$ ) sets most of the value of  $\gamma_3$ . Only when the spin is oriented along the valley axis ( $\hat{s} = \hat{\lambda}$ ), is this parameter excluded from the opposite-spin components of  $\mathbf{C}'_3(\mathbf{k}, \uparrow_s)$  [i.e., from the  $f_\pm(\mathbf{k})$  terms in Eq. (26)]. It will be shown that this behavior has important consequences on the anisotropy of intravalley spin relaxation.

*Connection between the L-point Hamiltonian parameters and spin relaxation.* To facilitate a connection between the Hamiltonian eigenvectors and spin relaxation we make use of spin-flip overlap integrals. We show that the direct spin-orbit coupling between the conduction bands ( $\Delta_L$ ) plays a key role in setting the intervalley spin relaxation rate (independently treated in Sec. III). On the other hand, we will see that intravalley spin-flip transitions are weaker. To make these

connections clear, we write the overlap integral

$$\mathcal{I}(\mathbf{k}, \mathbf{s}; \mathbf{k}', -\mathbf{s}) = \sum_{\mu, \gamma} \langle \mathbf{L}_{\mu, \mathbf{k}_L} | \mathbf{C}_\mu^\dagger(\mathbf{k}', -\mathbf{s}) \mathbf{C}_\gamma(\mathbf{k}, \mathbf{s}) | \mathbf{L}_{\gamma, \mathbf{k}_L} \rangle, \quad (29)$$

where  $\mathbf{k}$  and  $\mathbf{k}'$  are measured from the nearby valley center ( $\mathbf{k}_L$  and  $\mathbf{k}'_L$ ). The *bra* and *ket* states of this overlap integral include only the periodic Bloch parts in Eq. (16). While the combined phase factor  $\exp\{i(\mathbf{k}_L - \mathbf{k}'_L + \mathbf{k} - \mathbf{k}') \cdot \mathbf{r}\}$  is excluded from the overlap integral, it will be taken into account in the phonon phase when calculating the matrix elements. Using Eq. (26), the overlap integrals of electrons in different valleys read ( $\mathbf{k}_L \neq \mathbf{k}'_L$ )

$$\begin{aligned} \mathcal{I}(\mathbf{k}, \mathbf{s}; \mathbf{k}', \mathbf{s}) &= c_{1, \mathbf{s}}, \\ \mathcal{I}(\mathbf{k}, \mathbf{s}; \mathbf{k}', -\mathbf{s}) &= c_{3, \mathbf{s}} \frac{\Delta_L}{E_{g,u}} + O(k^2), \end{aligned} \quad (30)$$

where  $c_{j, \mathbf{s}}$  are constants of order unity that denote contributions from the spin-orientation dependence ( $\hat{s}$ ) and from the overlap of conduction basis states in different valleys:  $\langle \mathbf{L}_{1, \mathbf{k}_L} | \mathbf{L}_{j, \mathbf{k}'_L} \rangle$ . Equation (30) implies that the ratio between spin and momentum relaxation rates due to intervalley scattering is about  $\Delta_L^2/E_{g,u}^2$  (independent of the values of the wave vectors with respect to the valley centers). For intravalley scattering ( $\mathbf{k}_L = \mathbf{k}'_L$ ), on the other hand, the basis functions are orthogonal:  $\langle \mathbf{L}_{\mu, \mathbf{k}_L}^n | \mathbf{L}_{\gamma, \mathbf{k}_L}^m \rangle = \delta_{\mu\gamma} \delta_{mn}$ . As a result, the spin-flip overlap integral for electrons of the same valley reads

$$\mathcal{I}_a(\mathbf{k}, \downarrow_\lambda; \mathbf{k}', \uparrow_\lambda) = \frac{2P^2}{E_{g,v}^2} (\gamma_2 q_+ K_\lambda + i \gamma_1 q_- K_-), \quad (31)$$

where  $\mathbf{q} = \mathbf{k} - \mathbf{k}'$ ,  $2\mathbf{K} = \mathbf{k} + \mathbf{k}'$ , and  $X_\pm = X_w \pm i X_u$ . The terms have quadratic wave vector dependence and they are proportional to the spin-orbit constants in Eq. (28).<sup>62</sup> The overlap integral of other spin orientations ( $\hat{s} \neq \hat{\lambda}$ ) will be discussed below.

### C. Intravalley spin relaxation

The power-law dependence of intravalley spin-flip matrix elements can be identified by their transformation properties under time-reversal and space-inversion operations. Yafet showed that spin-flip matrix elements due to scattering with long-wavelength acoustic phonons have a cubic (quadratic) wave vector dependence in Ge (Si).<sup>42</sup> In Appendix D these important findings are generalized and it is shown that in Ge  $M_\lambda(\mathbf{k}, \mathbf{s}; \mathbf{k}', -\mathbf{s})$  scales with  $K_\ell q_m q_n$  for scattering with acoustic phonon modes ( $\lambda = \text{LA}$  or  $\text{TA}$ ) and with  $K_\ell q_m$  for optical phonon modes ( $\lambda = \text{LO}$  or  $\text{TO}$ ).  $\mathbf{K}$  and  $\mathbf{q}$  are, respectively, the average and difference of  $\mathbf{k}$  and  $\mathbf{k}'$ . For intravalley scattering in Si the  $\mathbf{K}$  dependence drops. We first explain this interesting difference.

From inspection of the wave vector dependence of intravalley spin flips in Ge ( $K_\ell q_m$  for optical modes and  $K_\ell q_m q_n$  for acoustic modes), one sees that they are forbidden between opposite points with respect to the valley center ( $\mathbf{K} = 0$ ). This restriction on spin-flip transitions is a manifestation of time-reversal symmetry. In silicon,  $\mathbf{K}$ -dependent scattering belongs to the intervalley  $g$  process which involves transitions between two valleys on opposite sides of the same crystal

axis.<sup>10,13</sup> Since in Ge the valley center is at the zone edge ( $L$  point), this type of scattering occurs within a single valley. Its dependence on the wave vector components ( $Kq^i$ ) amounts to the combined effects of intervalley  $g$  process and intravalley scattering in Si ( $K$  and  $q^i$ ).

Beyond the power-law dependence, an analytical approach to derive accurate intravalley matrix elements requires a combination of  $\mathbf{k} \cdot \mathbf{p}$ , rigid-ion and group theories.<sup>13</sup> Because of the wave vector dependence of these matrix elements, one cannot invoke group theory alone to find their exact forms (as we did for zeroth-order intervalley spin flips). We employ a simpler approach than in Ref. 13 and describe the interaction with long-wavelength acoustic phonons by  $H_{\text{intra}}^{\text{TA/LA}} = \Xi q$ , where  $\Xi$  is an effective deformation potential constant.<sup>10,60</sup> This scalar form averages out the scattering angle dependence of the second-rank deformation potential tensor.<sup>46</sup> We do not model the electron scattering with long-wavelength optical phonons since it is a weak effect in nonpolar semiconductors.<sup>60,63</sup>

We use selection rules of the  $L$ -point space group to construct the spin-flip matrix element from the overlap integral. The transformation property of the deformation potential tensor  $L'_3 \otimes L'_3 = L_1 + L_2 + L_3$  implies that direct coupling of conduction and valence states is excluded because of their opposite parities ( $L_1 \otimes L'_3 = L'_3$ ). This tensor can, however, couple any of the basis states to themselves ( $L_i \otimes L_i$ ). This behavior justifies the use of the spin-flip overlap integral. The resulting intravalley spin-flip matrix element in the  $L_{111}$  valley is approximated by

$$M_\lambda(\mathbf{k}, \mathbf{s}; \mathbf{k}', -\mathbf{s}) \approx \Xi q \mathcal{I}_a(\mathbf{k}, \mathbf{s}; \mathbf{k}', -\mathbf{s}), \quad (32)$$

where  $\lambda$  denotes any of the long-wavelength acoustic modes (TA or LA). Following a straightforward procedure we find

$$\mathcal{I}_a(\mathbf{k}, \mathbf{s}; \mathbf{k}', -\mathbf{s}) = i \sin \vartheta A_t + A_l \cos^2 \frac{\vartheta}{2} + A_l^* \sin^2 \frac{\vartheta}{2}, \quad (33)$$

where  $\cos \vartheta = \mathbf{s} \cdot \hat{\lambda}$  and

$$\begin{aligned} A_t &= \frac{i}{2} (\mathcal{I}_a(\mathbf{k}, \uparrow_\Lambda; \mathbf{k}', \uparrow_\Lambda) - \mathcal{I}_a(\mathbf{k}, \downarrow_\Lambda; \mathbf{k}', \downarrow_\Lambda)) \\ &= \frac{2P^2}{E_{g,v}^2} \gamma_3 (\mathbf{K} \times \mathbf{q})_\Lambda, \\ A_l &= e^{-i\varphi} \mathcal{I}_a(\mathbf{k}, \downarrow_\Lambda; \mathbf{k}', \uparrow_\Lambda) \\ &= \frac{2P^2}{E_{g,v}^2} (\gamma_2 q_+ K_\Lambda + i \gamma_1 q_- K_-) e^{-i\varphi}. \end{aligned} \quad (34)$$

$\varphi$  is the azimuthal angle of  $\mathbf{s}$  measured with respect to the  $w$  axis in the  $wu$  plane. Most importantly,  $\gamma_3$ , which incorporates the effect of the internal spin-orbit coupling in the valence band [Eq. (28c)], does not affect the spin-flip amplitude [Eq. (32)] when the spin orientation is along the valley axis ( $\vartheta = 0$ ). This effect leads to a pronounced anisotropy in the intravalley spin lifetime.

It is not surprising that the overlap integral approach yields correct wave vector power-law dependence [substituting Eqs. (33) and (34) into Eq. (32)]. The space-inversion and time-reversal symmetries are respected by the Hamiltonian whose eigenvectors were used to calculate the intravalley spin-flip overlap integral. These symmetries also lead to the

so-called Elliott-Yafet cancellation of all terms up to quadratic order in  $\mathbf{q}$ .<sup>13,42</sup> In fact, since the Hamiltonian respects all other symmetries of the  $L$ -point space group, the intravalley matrix element shows other selection rules.<sup>64</sup> From Eq. (34) we see, for example, that a spin flip is forbidden when the electron is scattered along the valley axis (i.e.,  $q_w = q_u = 0$ ,  $q_\Lambda \neq 0$ ). This constraint is understood by the symmetry of the vector-type coupling with the valence states ( $L_1 \otimes L'_3 = L'_3$ ). As mentioned, this coupling involves the two transverse components ( $\hat{\mathbf{w}}$  and  $\hat{\mathbf{u}}$ ) with respect to the valley axis ( $\hat{\Lambda}$ ).

We calculate the spin lifetime in the  $L_{111}$  valley due to electron scattering with long-wavelength acoustic phonon modes. This intravalley process dominates the intrinsic spin relaxation under conditions of [111] strain.<sup>12</sup> For sufficient uniaxial compressive strain along this direction ( $\sim 1\%$ ), one of the valleys is significantly lowered in energy and the intervalley scattering is quenched. Then, phonon-induced intravalley spin flips can dictate the spin relaxation of conduction electrons if scattering from impurities is negligible (nondegenerate doping). To get an analytical expression of the intravalley spin lifetime, the phonon energy is approximated by  $\Omega_{\text{ac}}(\mathbf{q}) = \hbar v_{\text{ac}} q$ , where  $v_{\text{ac}} \simeq 3.5 \times 10^5$  cm/s is the speed of acoustic phonons in Ge. We also make use of the long-wavelength limit and approximate the acoustic phonon population by  $k_B T / \Omega_{\text{ac}}(\mathbf{q}) \gg 1$ . Then by considering a Boltzmann distribution of electrons and substituting Eqs. (32)–(34) into Eq. (4) one gets

$$\frac{1}{\tau_{s,\text{intra}}} = \frac{\gamma_3^2}{\tau_0} \left( \frac{k_B T}{U_0} \right)^{\frac{7}{2}} [\sin^2 \vartheta + (1 + \cos^2 \vartheta) \beta], \quad (35)$$

where  $U_0 = 25.85$  meV is the room-temperature thermal energy.  $\beta \approx 0.12$  and  $\tau_0 \approx 0.3$  ns are expressed by

$$\beta = \frac{2m_l \gamma_2^2 + 3m_t \gamma_1^2}{5m_t \gamma_3^2}, \quad (36)$$

$$\frac{1}{\tau_0} = \frac{1024}{3} \left( 1 - \frac{m_t}{m_t^*} \right)^2 \frac{\Xi^2}{E_{g,v}^2} \left( \frac{m_d}{2\pi} \right)^{\frac{3}{2}} \frac{U_0^{\frac{7}{2}}}{\hbar^4 \rho v_{\text{ac}}^2}. \quad (37)$$

In accord with momentum scattering, we have used a value of  $\Xi = 7.5$  eV for the deformation potential constant.<sup>60</sup> The anisotropy in the intravalley spin relaxation is evident [square bracket term in Eq. (35)]. Our analysis shows that the lifetime is the longest for spin orientation along the valley (and strain) axis where  $\vartheta = 0$ . It drops by nearly a factor of 5 when the spin is oriented in the perpendicular plane ( $\vartheta = \pi/2$ ). At room temperature this change amounts to reducing the intravalley spin lifetime from  $\sim 700$  to  $\sim 150$  ns. These extremely long time scales are a consequence of the space-inversion symmetry and the position of the valley center in the edge of the Brillouin zone.

The dashed line in Fig. 4 shows the calculated temperature dependence of the intrinsic spin lifetime due to intravalley scattering with long-wavelength acoustic phonons. The spin orientation is chosen along the  $z$  axis [assigning  $\cos^2 \vartheta = 1/3$  in Eq. (35)], and is therefore equivalent in all four valleys. Figure 4 also shows that in unstrained bulk Ge, the spin lifetime of conduction electrons due to intravalley scattering with acoustic phonons is two orders of magnitude longer than the intervalley spin lifetime at room temperature. In addition, at very low temperatures the intrinsic spin lifetime reaches time

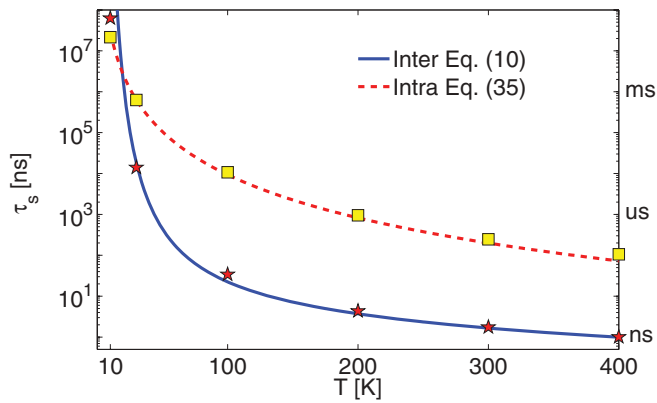


FIG. 4. (Color online) Calculated temperature dependence of the intrinsic spin lifetime in unstrained Ge due to electron-phonon interaction. The dashed line denotes the effect of intravalley scattering with long-wavelength acoustic phonons [Eq. (35)] for spin orientation along the  $z$  axis. The solid line denotes the much stronger effect of intervalley scattering in the unstrained case (Fig. 2). The markers are from rigorous numerical results (see Appendix B). To the best of our knowledge, the only available measured spin lifetime in nondegenerate bulk Ge above liquid He temperatures was recently reported by Guite and Venkataraman, where it was found that  $\tau_s = 4.6 \pm 1$  ns.<sup>32</sup> This result is in excellent agreement with the calculated spin lifetime, which in this temperature range is attributed to intervalley scattering. The rarity of experimental results, however, calls for additional measurements to fully test our theory.

scales of 1 s. Therefore, the phonon-induced spin relaxation is likely to be readily masked at very low temperatures by hyperfine interactions and Raman processes that are caused by *extrinsic* effects (e.g., electron localization on residual impurities).<sup>13</sup> Finally, the square markers in Fig. 4 show results of rigorous numerical calculations following the procedure in Ref. 9. Details of this numerical technique are provided in Appendix B. Evidently, the analytical approach of using overlap integrals provides rather accurate results and yet it clearly explains the underlying physics.

Before concluding this part, we compare three aspects of the intravalley spin relaxation in Si and Ge. First, the overlap integral approach is valid in Ge due to the relatively large separation of the nondegenerate conduction band from other valence and conduction bands. In Si, on the other hand, the intravalley spin relaxation is affected by the proximity of the conduction bands where the off-diagonal terms of the deformation potential play a key role.<sup>10,13</sup> Second, along the  $\Delta$ -symmetry axis which is relevant in Si, the spin-orbit coupling does not lift the energy degeneracy between the upper pair of valence bands. As a result, the intravalley spin relaxation is not affected by the internal spin-orbit coupling in the valence band and the anisotropy is weaker in Si reaching a factor of 2.<sup>13</sup> Finally, the intrinsic spin relaxation rate of the intravalley process exceeds that of the intervalley process below 50 K in Si,<sup>65</sup> and below 20 K in Ge. Reasons for the difference are the larger energy of zone-edge phonons in Si and the  $T^{5/2}$  rather than  $T^{7/2}$  temperature dependence of its intravalley process.

## V. SUMMARY

We have presented various origins that limit the intrinsic spin lifetime of conduction electrons in Ge. In unstrained bulk Ge and at  $T > 20$  K, the intrinsic spin lifetime is limited by intervalley electron scattering with zone-edge phonon modes of  $X_1$  and  $X_4$  symmetries (reaching  $\sim 1$  ns at 300 K). This spin lifetime is governed by the coupling with the upper conduction bands and its temperature dependence is set by the thermal population of the zone-edge phonons (with energies of about 30 meV). By analyzing time-reversal and crystal symmetries in the multivalley conduction band, we have found the spin orientation dependence of the dominant intervalley spin-flip processes. This dependence allowed us to quantify the change in the intervalley spin lifetime when varying the spin orientation under various stress configurations [Eqs. (10)–(13)].

We have derived a spin-dependent  $\mathbf{k}\cdot\mathbf{p}$  Hamiltonian model in the vicinity of the zone-edge  $L$  point [Eqs. (18)–(24)]. This compact model provides a lucid picture of the spin-orbit coupling effects in Ge. Similar to using the Kane model in zinc-blend semiconductors,<sup>66</sup> the compact  $L$ -point Hamiltonian has implications beyond derivation of spin-flip matrix elements. For example, by employing a plane-wave expansion along confined directions in nanostructures, this Hamiltonian model can be used to study spin-dependent properties in Ge nanostructures. Together with Si related theories,<sup>10,13</sup> one can also investigate spin properties in SiGe alloys.

Using the eigenvectors of the Hamiltonian matrix, we have derived forms of the spin-flip matrix elements due to intravalley scattering with long-wavelength acoustic phonons [Eqs. (32)–(34)]. The intrinsic spin relaxation rate of the intravalley process is found two orders of magnitude slower than that of the intervalley process. As such, intravalley spin flips affect the overall spin relaxation only when quenching the intervalley spin relaxation (e.g., by application of a uniaxial compressive stress along the [111] crystallographic axis).<sup>12</sup> Beyond the  $T^{7/2}$  temperature dependence of the intravalley spin relaxation, we have also quantified its dependence on the spin orientation [Eq. (35)]. The anisotropy of the intravalley spin relaxation results in a remarkably long spin lifetime (nearly 1  $\mu$ s at room temperature) when the spin is oriented along the valley (and strain) axis. The relatively large anisotropy of the intravalley spin relaxation was explained by the coupling with the internal spin-orbit interaction in the valence band.

We have elucidated the differences in the spin relaxation of bulk Si and Ge crystals. While both materials have a diamond-crystal structure, in Ge the valley center is located on the edge of the Brillouin zone ( $L$  point) and the lowest conduction band is well separated from other bands. These properties lead to a very long intravalley spin lifetime in Ge with a cubic power-law dependence of intravalley spin flips on wave vector components. This cubic dependence is also expected to be larger than in graphene where unlike Ge but similar to Si, the time-reversal operation couples states in inequivalent valleys. Therefore, in spite of being heavier than Si and carbon, nondegenerate and strained bulk Ge is a very promising material choice for implementing spintronic devices.<sup>67–70</sup>

**ACKNOWLEDGMENTS**

This work is supported by AFOSR Contract No. FA9550-09-1-0493 and by NSF Contract No. ECCS-0824075.

**APPENDIX A: DERIVATION OF THE SELECTION RULES FOR INTERVALLEY SPIN-FLIP TRANSITION**

We first focus on scattering between the  $L_{111}$  and  $L_{1\bar{1}\bar{1}}$  valley centers [ $\mathbf{k}_L = (1, 1, 1)/2$  and  $\mathbf{k}_{L_t} = (1, 1, -1)/2$ ]. Generalization to other valley centers is made at the end of this Appendix.

The selection rules connecting  $L$  and  $L_t$  points involve common symmetry operations of the little groups at  $\mathbf{k}_L$ ,  $-\mathbf{k}_{L_t}$ , and  $\mathbf{q}_X = \mathbf{k}_{L_t} - \mathbf{k}_L$ ,

$$g_c \in \{(\epsilon|0), (\bar{\epsilon}|0), (\delta_{2x\bar{y}}|\tau), (\bar{\delta}_{2x\bar{y}}|\tau), (i|\tau), (\bar{i}|\tau), (\rho_{x\bar{y}}|0), (\bar{\rho}_{x\bar{y}}|0)\}. \quad (\text{A1})$$

They also involve operations that switch between  $\mathbf{k}_L$  and  $-\mathbf{k}_{L_t}$ ,

$$g_e \in \{(\delta_{2z}|0), (\bar{\delta}_{2z}|0), (\rho_z|\tau), (\bar{\rho}_z|\tau), (\rho_{xy}|0), (\bar{\rho}_{xy}|0), (\delta_{2xy}|\tau), (\bar{\delta}_{2xy}|\tau)\}. \quad (\text{A2})$$

The bar over operations denotes an additional  $2\pi$  rotation (in double group notation). Table II lists the characters of the nontrivial operations. By considering these operations and time-reversal symmetry, the number of independent nonvanishing matrix elements for each of the zone-edge phonon symmetries in diamond-crystal structures ( $X_1$ ,  $X_3$ ,  $X_4$ ) is given by

$$\mathcal{N}_{X_i} = \frac{1}{2h_0} \left[ \sum_{g_c} \chi_{L_{6i}^+}^{-\mathbf{k}_{L_t}}(g_c) \chi_{L_6^+}^{\mathbf{k}_L}(g_c) \chi_{X_i}^{\mathbf{q}_X}(g_c) - \sum_{g_e} \chi_{L_6^+}^{\mathbf{k}_L}(g_e) \chi_{X_i}^{\mathbf{q}_X}(g_e) \right], \quad (\text{A3})$$

TABLE II. Nontrivial relevant IR characters and matrices in an intervalley scattering between  $\mathbf{k}_L$  and  $\mathbf{k}_{L_t}$  valleys. For 1D IR  $L_{1(t)}$  and 2D IR  $X_3$  only characters are used and shown.  $I$  and  $\sigma_x$  used in 2D IR  $X_1$  and  $X_4$  are the  $2 \times 2$  identity matrix and Pauli matrix. These matrices are based on our choice of basis states. The final results do not depend on this specific choice since the two phonon modes belonging to each IR are degenerate.  $\chi_{L_t}^{-\mathbf{k}_{L_t}} = \chi_{L_t}^{\mathbf{k}_{L_t}}$ . Also shown is the effect of exchange operations on  $L$  star. Basis states in  $D_{1/2}$  is along  $\pm z$  in spin space.

	$X_1$	$X_3$	$X_4$	$L_1$	$L_{1t}$	$D_{1/2}$
$(\delta_{2x\bar{y}} \tau)$	$\sigma_x$	$-I$	$I$	1	-1	$e^{-\frac{3\pi i}{4}} \begin{pmatrix} 0 & i \\ 1 & 0 \end{pmatrix}$
$(i \tau)$	$\sigma_x$	0	$\sigma_x$	1	-1	$\begin{pmatrix} 1 & 0 \\ 0 & 1 \end{pmatrix}$
$(\rho_{x\bar{y}} 0)$	$I$	0	$\sigma_x$	1	1	$e^{-\frac{3\pi i}{4}} \begin{pmatrix} 0 & i \\ 1 & 0 \end{pmatrix}$
$(\delta_{2z} 0)$	$I$	-2	$-I$	$\mathbf{k}_L \leftrightarrow -\mathbf{k}_{L_t}$		$\begin{pmatrix} -i & 0 \\ 0 & i \end{pmatrix}$
$(\rho_z \tau)$	$\sigma_x$	0	$-\sigma_x$	$\mathbf{k}_L \leftrightarrow -\mathbf{k}_{L_t}$		$\begin{pmatrix} -i & 0 \\ 0 & i \end{pmatrix}$
$(\rho_{xy} 0)$	$I$	0	$-\sigma_x$	$\mathbf{k}_L \leftrightarrow -\mathbf{k}_{L_t}$		$e^{-\frac{3\pi i}{4}} \begin{pmatrix} 0 & 1 \\ i & 0 \end{pmatrix}$
$(\delta_{2xy} \tau)$	$\sigma_x$	-2	$I$	$\mathbf{k}_L \leftrightarrow -\mathbf{k}_{L_t}$		$e^{-\frac{3\pi i}{4}} \begin{pmatrix} 0 & 1 \\ i & 0 \end{pmatrix}$

where  $h_0 = 8$  is the number of  $g_c$  or  $g_e$  operations and  $\chi_{L_{6i}^+} = \chi_{L_{1(t)}} \times \chi_{1/2}$ . The second sum in Eq. (A3) denotes the effect of time-reversal symmetry and the minus sign takes into account the parity from the spinor basis and electron-phonon interaction (see Ref. 46 for more details). By straightforwardly plugging the characters of Table II into Eq. (A3) one finds the general selection rule of Eq. (8).

Our aim is to express matrix elements of intervalley electron scattering with  $X$  point zone-edge phonons,

$$M_{X_i}(\mathbf{k}_L, \mathbf{s}_1; \mathbf{k}_{L_t}, \mathbf{s}_2) \equiv \langle \mathbf{k}_{L_t}, \mathbf{s}_2 | H_{X_i} | \mathbf{k}_L, \mathbf{s}_1 \rangle, \quad (\text{A4})$$

in terms of  $\mathcal{N}_{X_i}$  independent constants. This identification is made by connecting different matrix elements via appropriate symmetry operations.

First, by time-reversal and space-inversion symmetries of diamond-crystal structures we can write

$$\langle \mathbf{k}_{L_t}, \uparrow | H_{X_i} | \mathbf{k}_L, \uparrow \rangle = \langle \mathbf{k}_{L_t}, \downarrow | H_{X_i} | \mathbf{k}_L, \downarrow \rangle^*, \quad (\text{A5})$$

$$\langle \mathbf{k}_{L_t}, \downarrow | H_{X_i} | \mathbf{k}_L, \uparrow \rangle = -\langle \mathbf{k}_{L_t}, \uparrow | H_{X_i} | \mathbf{k}_L, \downarrow \rangle^*. \quad (\text{A6})$$

These identities hold for all phonons and possible spin orientations. The minus sign in Eq. (A6) roots from the Pauli matrix  $\sigma_y$  in the time-reversal operator  $\hat{T} = \hat{K} \sigma_y$ , where  $\hat{K}$  is the complex conjugate operator.

We first study the case  $\mathbf{s} \parallel \mathbf{z}$ , where  $\mathbf{s}$  is the spin orientation. For  $X_1$ , the  $(\rho_{x\bar{y}}|0)$  operation equates spin-conserving transition to itself (seen from the IR matrices of  $X_1$  and  $D_{L_{6i}^+} = D_{L_{1(t)}} \times D_{1/2}$  in Table II),

$$\langle \mathbf{k}_{L_t}, \uparrow | H_{X_1^{a(b)}} | \mathbf{k}_L, \uparrow \rangle \stackrel{(\rho_{x\bar{y}}|0)}{=} \langle \mathbf{k}_{L_t}, \downarrow | H_{X_1^{a(b)}} | \mathbf{k}_L, \downarrow \rangle, \quad (\text{A7})$$

where two  $X_1$  basis states are denoted as  $X_1^a$  and  $X_1^b$ . This choice is arbitrary and will not affect the final results due to the twofold degeneracy of the phonon modes. Equations (A5) and (A7) require the matrix elements of each of the  $X_1$  phonon branches to be a real number. From Table II one can also find  $(i|\tau)$  relates the matrix elements of the two degenerate modes by a minus sign,

$$\langle \mathbf{k}_{L_t}, \uparrow | H_{X_1^{a(b)}} | \mathbf{k}_L, \uparrow \rangle \stackrel{(i|\tau)}{=} -\langle \mathbf{k}_{L_t}, \uparrow | H_{X_1^{b(a)}} | \mathbf{k}_L, \uparrow \rangle. \quad (\text{A8})$$

With this additional information, a real number  $D_{X_1, m}$  could be assigned such that

$$\langle \mathbf{k}_{L_t}, \uparrow | H_{X_1^a} | \mathbf{k}_L, \uparrow \rangle = -\langle \mathbf{k}_{L_t}, \uparrow | H_{X_1^b} | \mathbf{k}_L, \uparrow \rangle = D_{X_1, m}. \quad (\text{A9})$$

Other operations do not give further information on these matrix elements.

With the same operations, the result for spin-flip transition is

$$\langle \mathbf{k}_{L_t}, \downarrow | H_{X_1^{a(b)}} | \mathbf{k}_L, \uparrow \rangle \stackrel{(\rho_{x\bar{y}}|0)}{=} -i \langle \mathbf{k}_{L_t}, \uparrow | H_{X_1^{a(b)}} | \mathbf{k}_L, \downarrow \rangle, \quad (\text{A10})$$

$$\langle \mathbf{k}_{L_t}, \downarrow | H_{X_1^{a(b)}} | \mathbf{k}_L, \uparrow \rangle \stackrel{(i|\tau)}{=} -\langle \mathbf{k}_{L_t}, \downarrow | H_{X_1^{a(b)}} | \mathbf{k}_L, \uparrow \rangle. \quad (\text{A11})$$

Together with Eq. (A6), we can assign a real number  $D_{X_{1,s}}$  such that

$$\begin{aligned} \langle \mathbf{k}_{L_t}, \downarrow | H_{X_1^a} | \mathbf{k}_L, \uparrow \rangle &= -\langle \mathbf{k}_{L_t}, \downarrow | H_{X_1^b} | \mathbf{k}_L, \uparrow \rangle \\ &= (1+i)D_{X_{1,s}}. \end{aligned} \quad (\text{A12})$$

Next we analyze matrix elements due to  $X_4$  modes, where there is only one independent scattering constant. From Table II the operations  $(\delta_{2x\bar{y}}|\tau)$  and  $(i|\tau)$  give relations for spin-conserving transitions

$$\langle \mathbf{k}_{L_t}, \uparrow | H_{X_4^{a(b)}} | \mathbf{k}_L, \uparrow \rangle \stackrel{(\delta_{2x\bar{y}}|\tau)}{=} -\langle \mathbf{k}_{L_t}, \downarrow | H_{X_4^{a(b)}} | \mathbf{k}_L, \downarrow \rangle, \quad (\text{A13})$$

$$\langle \mathbf{k}_{L_t}, \uparrow | H_{X_4^{a(b)}} | \mathbf{k}_L, \uparrow \rangle \stackrel{(i|\tau)}{=} -\langle \mathbf{k}_{L_t}, \uparrow | H_{X_4^{b(a)}} | \mathbf{k}_L, \uparrow \rangle. \quad (\text{A14})$$

Together with Eq. (A5), a real number  $D_{X_{4,s}}$  could be assigned

$$\langle \mathbf{k}_{L_t}, \uparrow | H_{X_4^a} | \mathbf{k}_L, \uparrow \rangle = -\langle \mathbf{k}_{L_t}, \uparrow | H_{X_4^b} | \mathbf{k}_L, \uparrow \rangle = iD_{X_{4,s}}. \quad (\text{A15})$$

For spin-flip transitions, the exchange operation  $(\delta_{2z}|0)$  together with the general time-reversal operation connect the matrix elements to their negatives,

$$\begin{aligned} \langle \mathbf{k}_{L_t}, \downarrow | H_{X_4^{a(b)}} | \mathbf{k}_L, \uparrow \rangle &\stackrel{(\delta_{2z}|0)}{=} \langle -\mathbf{k}_L, \downarrow | H_{X_4^{a(b)}} | -\mathbf{k}_{L_t}, \uparrow \rangle \\ &\stackrel{\text{TR}}{=} -\langle \mathbf{k}_{L_t}, \downarrow | H_{X_4^{a(b)}} | \mathbf{k}_L, \uparrow \rangle, \end{aligned} \quad (\text{A16})$$

where the time-reversal operation sends electron states to their Kramers conjugate, and keeps the electron-phonon interaction. Thus spin-flip matrix elements due to  $X_4$  phonon modes vanish.

Therefore, with spin direction along  $z$ , the scattering matrices from  $\mathbf{k}_L$  to  $\mathbf{k}_{L_t}$  for relevant phonon modes are

$$H_{X_1^a} = -H_{X_1^b} = \begin{pmatrix} D_{X_{1,m}} & (-1+i)D_{X_{1,s}} \\ (1+i)D_{X_{1,s}} & D_{X_{1,m}} \end{pmatrix}, \quad (\text{A17})$$

$$H_{X_4^a} = -H_{X_4^b} = \begin{pmatrix} iD_{X_{4,s}} & 0 \\ 0 & -iD_{X_{4,s}} \end{pmatrix}, \quad (\text{A18})$$

where Eqs. (A5) and (A6) are used to get two other elements in each matrix. Equations (A17) and (A18) indicate that in this specific case  $X_1$  is allowed for both spin-conserving and spin-flip transitions, while  $X_4$  is only allowed for spin-conserving transition.

Next we extend the analysis to arbitrary spin orientation, which leads to the anisotropy of spin relaxation processes and enables a direct comparison to a wide range of spin injection experiments. The spin orientation ( $\mathbf{s}$ ) is defined in terms of polar ( $\theta$ ) and azimuthal angles ( $\phi$ ) with respect to the  $+z$  and  $+x$  directions. The new spin states relate to the original ones by an ‘‘active’’ rotation matrix in spin subspace,

$$\exp\left(\frac{i\boldsymbol{\sigma} \cdot \hat{\boldsymbol{\omega}}\theta}{2}\right) = \begin{pmatrix} \cos\frac{\theta}{2} & -\sin\frac{\theta}{2}e^{-i\phi} \\ \sin\frac{\theta}{2}e^{i\phi} & \cos\frac{\theta}{2} \end{pmatrix}, \quad (\text{A19})$$

where  $\hat{\boldsymbol{\omega}} = \hat{\mathbf{s}} \times \hat{\mathbf{z}} / |\hat{\mathbf{s}} \times \hat{\mathbf{z}}|$  is the unit vector along the rotation axis. The new spin states follow:

$$|\mathbf{k}_L, \uparrow\rangle = \cos\frac{\theta}{2}|\mathbf{k}_L, \uparrow_z\rangle + \sin\frac{\theta}{2}e^{i\phi}|\mathbf{k}_L, \downarrow_z\rangle, \quad (\text{A20})$$

TABLE III.  $|M_{X_i}(\mathbf{k}_L, \mathbf{s}; \mathbf{k}_{L_t}, -\mathbf{s})|^2/2D_{X_i}^2$  for intervalley spin flips between  $L_{111}$  and  $L_{1\bar{1}\bar{1}}$  valleys. For each of the nonvanishing modes  $X_i$ , the relative amplitude is provided for spin orientation ( $\mathbf{s}$ ) along any of the inequivalent high-symmetry crystal directions. Results between other valleys can all be obtained by trivial rotation transformation.

$\mathbf{s}$	[0 0 1]	[1 0 0]	[1 1 0]	[1 $\bar{1}$ 0]	[1 0 1]	[1 1 1]	[1 $\bar{1}$ 1]
$X_1$	4	2	4	0	3	4	4/3
$X_4$	0	2	2	2	1	4/3	4/3

$$|\mathbf{k}_L, \downarrow\rangle = -\sin\frac{\theta}{2}e^{-i\phi}|\mathbf{k}_L, \uparrow_z\rangle + \cos\frac{\theta}{2}|\mathbf{k}_L, \downarrow_z\rangle, \quad (\text{A21})$$

while the new scattering matrices from  $\mathbf{k}_L$  to  $\mathbf{k}_{L_t}$  are readily obtained by applying the rotation operator of Eq. (A19) on the matrices Eqs. (A17) and (A18). The new spin-flip matrix elements are

$$\begin{aligned} \langle \mathbf{k}_{L_t}, \downarrow | H_{X_1^a} | \mathbf{k}_L, \uparrow \rangle &= -\langle \mathbf{k}_{L_t}, \downarrow | H_{X_1^b} | \mathbf{k}_L, \uparrow \rangle \\ &= \left[ (1+i)\cos^2\frac{\theta}{2} + (1-i)\sin^2\frac{\theta}{2}e^{2i\phi} \right] D_{X_{1,s}}, \end{aligned} \quad (\text{A22})$$

$$\begin{aligned} \langle \mathbf{k}_{L_t}, \downarrow | H_{X_4^a} | \mathbf{k}_L, \uparrow \rangle &= -\langle \mathbf{k}_{L_t}, \downarrow | H_{X_4^b} | \mathbf{k}_L, \uparrow \rangle \\ &= i\sin\theta e^{i\phi} D_{X_{4,s}}. \end{aligned} \quad (\text{A23})$$

Summing the square amplitudes of the two branches leads to Eq. (9) in the paper. Table III lists the relative magnitudes of the squared spin-flip matrix elements for  $\mathbf{s}$  along several inequivalent high-symmetry directions of the crystal.

The matrix elements are determined by the relevant directions of the spin orientation and the valley-to-valley configurations. For configurations other than  $L_{111} \leftrightarrow L_{1\bar{1}\bar{1}}$ , the matrix elements could be obtained from Eq. (9) by coordinate transformations. If we rewrite Eq. (9) in the form of the projections of  $\mathbf{s}$  on  $x, y, z$  axes as

$$\begin{aligned} \sum_{i=1,2} |\langle \mathbf{k}_{L_t}, \downarrow | H_{X_i^j} | \mathbf{k}_L, \uparrow \rangle|^2 &= \begin{cases} 2D_{X_{1,s}}^2(1 + \hat{z}^2 + 2\hat{x}\hat{y}) & \text{if } j = 1 \\ 2D_{X_{4,s}}^2(1 - \hat{z}^2) & \text{if } j = 4 \end{cases}, \end{aligned} \quad (\text{A24})$$

then in other valley-to-valley configurations, for example,  $L_{\bar{1}\bar{1}\bar{1}} \leftrightarrow L_{1\bar{1}\bar{1}}$ , the matrix elements are just interchange  $\{\hat{x}, \hat{y}, \hat{z}\}$  of Eq. (A24) into  $\{\hat{x}, -\hat{z}, \hat{y}\}$ . Results of all possible configurations are listed in Table I of the paper.

## APPENDIX B: CALCULATING VALUES OF MATRIX ELEMENTS AND OF INTERVALLEY SPIN-FLIP SCATTERING CONSTANTS

We present the procedure to numerically calculate the values of spin-flip matrix elements  $[M_\nu(\mathbf{k}_1, \uparrow; \mathbf{k}_2, \downarrow)]$  and of the intervalley spin-flip scattering  $[D_{X_{1,s}}$  and  $D_{X_{4,s}}$  in Eq. (9)]. These results are then used to calculate the spin lifetime using a numerical technique that is briefly discussed at the end of this Appendix. The *bra* and *ket* states in matrix elements are taken from the results of a local empirical pseudopotential method

(EPM) where spin-dependent states have the form<sup>59</sup>

$$\begin{aligned}
 |\mathbf{k}, \uparrow, \ell\rangle &= \exp(i\mathbf{k} \cdot \mathbf{r}) \sum_{\mathbf{g}_j}^{N_g} C_{\mathbf{g}_j}(\mathbf{k}, \uparrow, \ell) \exp(i\mathbf{g}_j \cdot \mathbf{r}), \\
 |\mathbf{k}, \downarrow, \ell\rangle &= \exp(i\mathbf{k} \cdot \mathbf{r}) \sum_{\mathbf{g}_j}^{N_g} C_{\mathbf{g}_j}(\mathbf{k}, \downarrow, \ell) \exp(i\mathbf{g}_j \cdot \mathbf{r}). \quad (\text{B1})
 \end{aligned}$$

The three quantum numbers of a state are the wave vector ( $\mathbf{k}$ ), band number ( $\ell$ ), and spin state ( $\uparrow$  or  $\downarrow$ ).  $\mathbf{g}_j$  runs over  $N_g$  reciprocal lattice vectors for each of the two spin species,

$$\begin{aligned}
 C_{\mathbf{g}_j}(\mathbf{k}, \uparrow, \ell) &= a_{\mathbf{g}_j}(\mathbf{k}, \ell)|\uparrow\rangle + b_{\mathbf{g}_j}(\mathbf{k}, \ell)|\downarrow\rangle, \\
 C_{\mathbf{g}_j}(\mathbf{k}, \downarrow, \ell) &= a_{\mathbf{g}_j}^*(\mathbf{k}, \ell)|\downarrow\rangle - b_{\mathbf{g}_j}^*(\mathbf{k}, \ell)|\uparrow\rangle. \quad (\text{B2})
 \end{aligned}$$

To find the  $a_{\mathbf{g}_j}(\mathbf{k}, \ell)$  and  $b_{\mathbf{g}_j}(\mathbf{k}, \ell)$  coefficients and to facilitate the calculation of matrix elements, we define a bare potential and spin-orbit coupling functions,

$$\mathcal{V}_+(\mathbf{k}) = [V_k \cos(\mathbf{k} \cdot \boldsymbol{\tau})] \mathcal{I}, \quad (\text{B3})$$

$$\mathcal{V}_{\text{so}}(\mathbf{k}_1, \mathbf{k}_2) = -i\mu_0 A(\mathbf{k}_1, \mathbf{k}_2) \cos(\Delta\mathbf{k} \cdot \boldsymbol{\tau}) \{\mathbf{k}_3 \cdot \boldsymbol{\sigma}\}. \quad (\text{B4})$$

$\pm\boldsymbol{\tau} = \pm(a, a, a)/8$  denotes positions of the two atoms in the unit cell where  $a$  is the lattice constant and the origin is the midpoint between the two atoms. The wave vector parameters are  $\Delta\mathbf{k} = \mathbf{k}_1 - \mathbf{k}_2$  and  $\mathbf{k}_3 = \mathbf{k}_1 \times \mathbf{k}_2$ .  $V_k$  is the form factor relating to the Fourier transform of the local atomic pseudopotential.  $A(\mathbf{k}_1, \mathbf{k}_2)$  and  $\mu_0$  denote spin-orbit coupling parameters which are set by the potential close to the atom cores. These three variables are discussed in greater detail below.

To account for scattering between arbitrary states, one needs to obtain the continuous curve of the form factor ( $V_k$ ). We have employed a piecewise Hermite cubic interpolation from empirical values of the form factor at the first few reciprocal lattice vectors and from its wave vector derivative at these points,

$$\begin{aligned}
 V_0 &= -0.558, & V_{\sqrt{3}} &= -0.288, & V_{\sqrt{8}} &= 0.029, \\
 V_{\sqrt{11}} &= 0.052, & V'_0 &= 0, & V'_{\sqrt{3}} &= 0.386, \\
 V'_{\sqrt{8}} &= 0.221, & V'_{\sqrt{11}} &= -0.066,
 \end{aligned}$$

where  $k$  is in units of  $2\pi/a$  and  $V_k$  in Ry. We also assume that  $V_{k>3.8} = 0$  in agreement with its negligible values in this wave vector range. All these values were chosen after careful calibration in which not only the band structure of Ge is recovered but also its deformation potential quantities (shifts of energy bands and changes of energy gaps with respect to stress). Given that a lattice vibration is essentially a dynamic stress, these quantities are imperative for scattering problems.

For the spin-orbit coupling parameters [Eq. (B4)] we have followed the analysis of section F in Ref. 59.  $A(\mathbf{K}_1, \mathbf{K}_2)$  is calculated from atomic radial functions using Herman-Skillman tables,<sup>71</sup> while  $\mu_0 = 11.3 \text{ meV } \text{\AA}^2$  is the only free parameter whose value is chosen to fit experimentally known parameters such as the split-off energy. An approximate but more compact approach to treat the atomic spin-orbit coupling follows Eq. (8) of Ref. 72 whose parameters for Ge are  $\mu = 12.25 \text{ meV}$  and  $\zeta = 10 \text{ \AA}^{-1}$ .

Using Eqs. (B3) and (B4), the wave function coefficients in Eq. (B2) are eigenvectors of a  $2N_g \times 2N_g$  Hamiltonian matrix constructed from the following  $2 \times 2$  blocks:<sup>59</sup>

$$\begin{aligned}
 \mathcal{H}_{\mathbf{g}_1, \mathbf{g}_2}(\mathbf{k}) &= \left( \frac{\hbar^2 |\mathbf{g}_1 + \mathbf{k}|^2}{2m^*} \delta_{\mathbf{g}_1, \mathbf{g}_2} \right) \mathcal{I} + \mathcal{V}_+(\Delta\mathbf{g}) \\
 &+ \mathcal{V}_{\text{so}}(\mathbf{K}_1, \mathbf{K}_2). \quad (\text{B5})
 \end{aligned}$$

$\Delta\mathbf{g} = \mathbf{g}_1 - \mathbf{g}_2$  and  $\mathbf{K}_{1(2)} = \mathbf{g}_{1(2)} + \mathbf{k}$ . In order to fit the band structure, we have used a plane-wave basis with  $N_g = 235$  reciprocal lattice vectors for each spin species and used  $m^* = 1.235m_0$  in the kinetic term of Eq. (B5). The resulting energy band structure is shown in Fig. 3.

Following Eq. (2) of the main text, the spin-flip matrix element reads

$$\begin{aligned}
 M_\nu(\mathbf{k}_1, \uparrow; \mathbf{k}_2, \downarrow) &= \sum_{j, \alpha} \xi_{\alpha, \nu}(\mathbf{q}) e^{i\mathbf{q}\mathbf{R}_{j\alpha}} \cdot \langle \mathbf{k}_2, \downarrow | \nabla_r \mathcal{V}_{\text{at}}(\mathbf{r} - \mathbf{R}_{j\alpha}) | \mathbf{k}_1, \uparrow \rangle, \quad (\text{B6})
 \end{aligned}$$

where the band index is omitted from the *bra* and *ket* states knowing that the scattering is between states of the lowest conduction band. The atom displacement vector  $[\xi_{\alpha, \nu}(\mathbf{q})]$  is calculated from a standard adiabatic bond-charge model in Ge, where we use without changing the force constants from Refs. 53 and 73, except that we set the convergence parameter to  $P = 0.25$  to achieve fast Ewald transformation. The number of reciprocal lattice vectors used is 59 and of real lattice vectors is 55.

The electron-phonon interaction matrix element in Eq. (B6) is easy to write down in terms of plane-wave basis states. Substituting Eqs. (B1)–(B4) into Eq. (B6) and changing the integration coordinates  $\mathbf{r} \rightarrow \mathbf{r} + \mathbf{R}_{j\alpha}$ , we get that

$$\begin{aligned}
 M_\nu(\mathbf{k}_1, \uparrow; \mathbf{k}_2, \downarrow) &= \sum_{\mathbf{g}_1, \mathbf{g}_2} \Delta\mathbf{K} \sum_{\alpha} \xi_{\alpha, \nu}(\mathbf{q}) C_{\mathbf{g}_2}^\dagger(\mathbf{k}_2, \downarrow) \\
 &\times [\mathcal{V}_+(\Delta\mathbf{K}) + \mathcal{V}_{\text{so}}(\mathbf{K}_1, \mathbf{K}_2)] C_{\mathbf{g}_1}(\mathbf{k}_1, \uparrow), \quad (\text{B7})
 \end{aligned}$$

where  $\mathbf{K}_{1(2)} = \mathbf{g}_{1(2)} + \mathbf{k}_{1(2)}$ ,  $\Delta\mathbf{K} = \mathbf{K}_2 - \mathbf{K}_1$ , and  $\mathbf{q} = \mathbf{k}_2 - \mathbf{k}_1$  is a result of the crystal translation symmetry. It is critical to use identical parameters in the electron-phonon interaction [Eq. (B7)] and in the Hamiltonian [Eq. (B5)]. This natural choice ensures the so called Elliott-Yafet cancellation,<sup>42</sup> in which intravalley spin-flip matrix elements in Ge vanish at the zeroth, first, and second powers of the wave vector components (see discussion in Appendix D). Using Eq. (B7), the bare potential part  $\mathcal{V}_+$  corresponds to *Elliott* processes in which spin flips are governed by coupling of opposite spin components in the state coefficients. The spin-orbit coupling part  $\mathcal{V}_{\text{so}}$  corresponds to the *Yafet* process in which spin flips are governed by  $\sigma_x$  and  $\sigma_y$  components of the spin-orbit coupling.

The intervalley spin-flip scattering constants  $D_{X_{1,s}}$  and  $D_{X_{4,s}}$  are calculated from Eq. (B7) by considering the  $\nu = X_1$  and  $\nu = X_4$  phonon symmetries with  $L$ -point states:  $\mathbf{k}_1 = \mathbf{k}_L$ ,  $\mathbf{k}_2 = \mathbf{k}_{Ll}$ , and  $\mathbf{q} = \mathbf{k}_{Ll} - \mathbf{k}_L$ . Using these phonon symmetries and wave vectors we get that  $D_{X_{1,s}} = 35 \text{ meV}/\text{\AA}$  and  $D_{X_{4,s}} = 46 \text{ meV}/\text{\AA}$ . When performing rigorous numerical integration of the spin lifetime [Eq. (4)], we have used a grid spacing of  $0.005 \times 2\pi/a$  in  $\mathbf{k}$  space while using Eq. (B7) to

TABLE IV. Relevant invariant components and matrices of the  $L_{111}$  point. The  $\{\Lambda, w, u\}$  are valley coordinates [Eq. (19)].

IRs	Invariant components (111)	Invariant matrices
$L_1$	$k^2, -\frac{1}{2}(k_w^2 + k_u^2) + k_\Lambda^2$	$1, I$
$L_2$	$\sigma_\Lambda$	$\rho_y$
$L_3$	$\{\sigma_w, \sigma_u\}$	$\{[0, 1], [1, 0]\}, \{\rho_x, \rho_z\}$
$L'_3$	$\{-k_w, k_u\}, \{(\mathbf{k} \times \boldsymbol{\sigma})_w, (\mathbf{k} \times \boldsymbol{\sigma})_u\}$	$\{[0, 1], [1, 0]\}$

calculate the spin-flip matrix elements for all possible  $\mathbf{k}_1$  and  $\mathbf{k}_2$  combinations up to state energies  $\sim 200$  meV above the conduction edge. These numerical results are shown by the marker symbols in Figs. 2 and 4.

### APPENDIX C: DERIVATION OF THE SPIN-DEPENDENT $L$ -POINT HAMILTONIAN AND CALCULATION OF ITS PARAMETERS

We use the method of invariants to derive the Hamiltonian. The general procedure is (1) figuring out the two IRs of the coupling matrix; (2) decomposing the direct product of these two IRs into a sum of IR(s); and (3) according to this decomposition, associating invariant components and matrices to construct the Hamiltonian. These invariant components and matrices are obtained by applying the symmetry operators on the components of the perturbation and the chosen basis states, respectively. Associating the invariants to IRs is then carried by examining the resulting transformation. Table IV lists these invariant components and matrices of the  $L_{111}$  point. From this table the constructions of  $H_{ij}$  in Eqs. (20)–(24) are straightforward.

Table V lists all of the calculated parameter constants that appear in the  $L$ -point Hamiltonian, where some values are also known empirically.<sup>57,74</sup> The energy gaps ( $E_{g,u}$  and  $E_{g,v}$ ), spin-orbit induced splitting ( $\Delta_3$  and  $\Delta_{3'}$ ), and masses are readily extracted from the spin-dependent band structure whose calculation details were discussed in Appendix B (the resulting energy bands are shown in Fig. 3). Interband parameters were calculated using a different technique which involves spin-independent states of different bands in the  $L$  point,

$$|\mathbf{k}_L, \ell\rangle = \exp(i\mathbf{k}_L \cdot \mathbf{r}) \sum_{\mathbf{g}_j}^{N_g} c_{\mathbf{g}_j}(\mathbf{k}, \ell) \exp(i\mathbf{g}_j \cdot \mathbf{r}), \quad (\text{C1})$$

where  $c_{\mathbf{g}_j}(\mathbf{k}, \ell)$  are elements of the eigenvectors of the spin-independent EPM Hamiltonian. Then, the evaluation of momentum matrix elements ( $P$ ,  $P_1$ , and  $P_2$  in Table V) follows

TABLE V. Parameters of the  $L$ -point Hamiltonian [Eqs. (20)–(24)] for bulk germanium.  $m_0$  denotes the free electron mass. See text for calculation details.

$E_{g,u}$	2.2	eV	$P$	9	eV $\text{\AA}$	$m_t^*$	$0.17m_0$
$E_{g,v}$	3.3	eV	$P_1$	7	eV $\text{\AA}$	$m_t^*$	$1.60m_0$
$\Delta_L$	0.027	eV	$P_2$	1.8	eV $\text{\AA}$	$m_{t,3}^*$	$1.2m_0$
$\Delta_3$	0.022	eV	$\alpha$	0.04	eV $\text{\AA}$	$m_{t,3}^*$	$1.7m_0$
$\Delta_{3'}$	0.1	eV				$m_{t,3'}^*$	$-0.16m_0$
						$m_{l,3'}^*$	$1.9m_0$

directly from

$$\mathbf{P} = \frac{\hbar^2}{m_0} \sum_{\mathbf{g}} \mathbf{g} c_{\mathbf{g}}^*(\mathbf{k}_L, \ell_i) c_{\mathbf{g}}(\mathbf{k}_L, \ell_j).$$

When calculating  $P$ ,  $\ell_i$  is the lowest conduction band,  $\ell_j$  is one of the doubly degenerate upper valence bands, and the nonvanishing components of  $\mathbf{g}$  are  $\{g_w, g_u\}$  ( $w$  and  $u$  are the transverse components lying perpendicular to the valley axis connecting the  $\Gamma$  and  $L$  points). When calculating  $P_1$  and  $P_2$ ,  $\ell_i$  and  $\ell_j$  are from the upper conduction and valence bands.  $P_1$  is evaluated with  $g_w$  and  $g_u$  while  $P_2$  with  $g_\Lambda$  (longitudinal component; along the valley axis).

The interband spin-orbit coupling parameters ( $\Delta_L$  and  $\alpha$ ) follow from the interaction of  $L$  states via  $\lambda[\nabla V \times (\mathbf{p} + \hbar\mathbf{k})]$ , where  $\lambda = \hbar/(4m_0^2c^2)$ . These constants are evaluated from

$$\sum_{\mathbf{g}_1, \mathbf{g}_2} [c_{\mathbf{g}_2}^*(\mathbf{k}_L, \ell_i) \mathbf{F}_{\text{so}} c_{\mathbf{g}_1}(\mathbf{k}_L, \ell_j)]. \quad (\text{C2})$$

In calculating  $\Delta_L$ , the spin-orbit coupling vector reads

$$\mathbf{F}_{\text{so}} = -i[\mu_0 A(\mathbf{K}_1, \mathbf{K}_2) \cos(\Delta\mathbf{g} \cdot \boldsymbol{\tau})] \mathbf{K}_1 \times \mathbf{K}_2, \quad (\text{C3})$$

where  $\mathbf{K}_i = \mathbf{g}_i + \mathbf{k}_L$ ,  $\Delta\mathbf{g} = \mathbf{g}_1 - \mathbf{g}_2$ , and other parameter are the same as in Eq. (B4). In addition, the involved bands [ $\ell_i$  and  $\ell_j$  in Eq. (C2)] are the lowest and upper conduction bands. In calculating  $\alpha$ , the involved bands are from the lowest conduction band and upper valence bands, while the spin-orbit coupling vector reads

$$\mathbf{F}_{\text{so}} = -i \frac{\mu_0}{k} [A(\mathbf{K}'_1, \mathbf{K}'_2) \cos(\Delta\mathbf{g} \cdot \boldsymbol{\tau}) \mathbf{K}'_1 \times \mathbf{K}'_2 - A(\mathbf{K}_1, \mathbf{K}_2) \cos(\Delta\mathbf{g} \cdot \boldsymbol{\tau}) \mathbf{K}_1 \times \mathbf{K}_2], \quad (\text{C4})$$

where  $\mathbf{K}'_i = \mathbf{g}_i + \mathbf{k}_L + \mathbf{k}$  and  $\mathbf{k}$  is measured from the  $L$  point along transverse axes ( $\mathbf{k} = k\hat{w}$  or  $\mathbf{k} = k\hat{u}$ ).

### APPENDIX D: WAVE VECTOR ORDER ANALYSIS OF INTRAVALLEY SPIN-FLIP TRANSITIONS

The theory for intravalley spin flips in Ge and Si share similar features. In Ref. 13 we have analyzed the case of Si. Here we summarize the important findings and discuss the difference for the case of Ge. By invoking space-inversion and time-reversal symmetries the leading order terms of intravalley scattering between  $|\mathbf{k}_1 = \mathbf{K} + \mathbf{q}/2, \uparrow\rangle$  and  $|\mathbf{k}_2 = \mathbf{K} - \mathbf{q}/2, \downarrow\rangle$  are found to be

$$\frac{\mathbf{q}^{\otimes 2}}{8} \langle \mathbf{K}, \downarrow | (\mathcal{L}^\dagger)^{\otimes 2} \mathcal{A}_{\mathbf{q}}^{+, \lambda} + \mathcal{A}_{\mathbf{q}}^{+, \lambda} \mathcal{L}^{\otimes 2} - 2\mathcal{L}^\dagger \mathcal{A}_{\mathbf{q}}^{+, \lambda} \mathcal{L} | \mathbf{K}, \uparrow \rangle + \frac{\mathbf{q}}{2} \langle \mathbf{K}, \downarrow | \mathcal{L}^\dagger \mathcal{A}_{\mathbf{q}}^{-, \lambda} + \mathcal{A}_{\mathbf{q}}^{-, \lambda} \mathcal{L} | \mathbf{K}, \uparrow \rangle, \quad (\text{D1})$$

where lower order terms (in  $\mathbf{q}$ ) vanish due to the celebrated Elliott-Yafet cancellation.<sup>13,42</sup> We explain the symbol notations of these matrix elements.  $\mathbf{q}^{\otimes 2} \cdot \mathcal{L}^{\otimes 2}$  denotes the scalar product of two second-rank tensors (each formed by a dyadic product of the vector with itself).  $\mathcal{L}$  is the derivative in  $\mathbf{k}$  space with its components defined by

$$\mathcal{L}_i |\mathbf{k}, \mathbf{s}\rangle \equiv \lim_{\delta\mathbf{k} \rightarrow 0} \frac{|\mathbf{k} + \delta k_i, \mathbf{s}\rangle - |\mathbf{k}, \mathbf{s}\rangle}{\delta k_i}. \quad (\text{D2})$$

In connection with the  $L$ -point Hamiltonian,  $\mathcal{L}$  operates on the eigenvectors  $[C_\gamma(\mathbf{k}, \mathbf{s})]$  and the envelope phase of the

wave function [ $\exp(i\mathbf{k} \cdot \mathbf{r})$ ]. The electron-phonon interaction in Eq. (D1) is given by

$$A_{\mathbf{q}}^{\pm, \lambda} = \xi_{\mathbf{q}}^{\pm, \lambda} \cdot \nabla \mathcal{V}_{\pm}, \quad (\text{D3})$$

where the  $+$  and  $-$  signs denote, respectively, the in-phase and out-of-phase motion of atoms in the unit cell. For scattering with long-wavelength acoustic phonon modes ( $\lambda$  is TA or LA), the out-of-phase polarization vector ( $\xi_{\mathbf{q}}^{-, \lambda}$ ) is linear in  $\mathbf{q}$ , while the in-phase vector ( $\xi_{\mathbf{q}}^{+, \lambda}$ ) has a zeroth-order dependence (e.g.,  $q_i/q$  terms). It is the opposite case for scattering with long-wavelength optical phonon modes ( $\lambda$  is TO or LO). These wave vector dependencies are taken into account in finding the power-law order of the intravalley spin-flip matrix element. Denoting the atoms' positions in the unit cell by  $\boldsymbol{\tau}_A$  and  $\boldsymbol{\tau}_B$  with respect to the cell's origin, the potential in Eq. (D3) reads

$$\mathcal{V}_{\pm}(\mathbf{r}) = \mathcal{V}_{\text{at}}(\mathbf{r} - \boldsymbol{\tau}_A) \pm \mathcal{V}_{\text{at}}(\mathbf{r} - \boldsymbol{\tau}_B), \quad (\text{D4})$$

where the spin-orbit interaction is included in the atomic potential [Eq. (3)].

In the next step of the analysis we expand the states around the valley center. The *bra* and *ket* states in Eq. (D1) are taken at the average of  $\mathbf{k}_1 = \mathbf{K} + \mathbf{q}/2$  and  $\mathbf{k}_2 = \mathbf{K} - \mathbf{q}/2$ . We expand

this averaged state around the valley center position ( $\mathbf{K}_0$ ),

$$|\mathbf{K}, \mathbf{s}\rangle = |\mathbf{K}_0, \mathbf{s}\rangle + \mathbf{K} \cdot \mathcal{L} |\mathbf{K}_0, \mathbf{s}\rangle + O(K^2), \quad (\text{D5})$$

where  $\mathbf{K}$  is measured with respect to  $\mathbf{K}_0$ . Substituting this expansion in Eq. (D1), one can identify which terms vanish. This identification is carried straightforwardly using the transformation properties of  $\mathcal{L}$ ,  $\nabla \mathcal{V}_{\pm}$ , and  $|\mathbf{K}_0, \mathbf{s}\rangle$  under space-inversion and time-reversal symmetries.

The difference between the analysis of Si and Ge stems from the position of the valley center. The valley center in Ge is at the zone-edge  $L$  point, and in Si it is inside the Brillouin zone ( $0.15 \times 2\pi/a$  away from the  $X$  point along the  $\Delta$  axis). Since  $\mathbf{K}_0$  and  $-\mathbf{K}_0$  are the same point in Ge, space-inversion operation keeps  $|\mathbf{K}_0, \mathbf{s}\rangle$  invariant in Ge but not in Si. Together with the transformations of  $\mathcal{L}$ ,  $\nabla \mathcal{V}_{\pm}$ , and  $|\mathbf{K}_0, \mathbf{s}\rangle$  one can readily identify the dominant contributions to intravalley spin-flip matrix elements. Scattering with long-wavelength acoustic phonons is led by  $q_{\ell}q_m$  products in Si and by  $K_{\ell}q_mq_n$  products in Ge. For scattering with long-wavelength optical phonons, the leading terms in Si are linear in  $\mathbf{q}$ , and in Ge they include  $K_{\ell}q_m$  products. Finding the exact products, their coefficients and deformation potential constants require a combination of  $\mathbf{k} \cdot \mathbf{p}$ , rigid ion, and group theories.<sup>13</sup>

\*pengke@ece.rochester.edu

†The first two authors have equal contribution to this work.

<sup>1</sup>B. E. Kane, *Nature (London)* **393**, 133 (1998).

<sup>2</sup>I. Žutić, J. Fabian, and S. Das Sarma, *Rev. Mod. Phys.* **76**, 323 (2004).

<sup>3</sup>I. Žutić, J. Fabian, and S. C. Erwin, *Phys. Rev. Lett.* **97**, 026602 (2006).

<sup>4</sup>H. Dery, P. Dalal, Ł. Cywiński, and L. J. Sham, *Nature (London)* **447**, 573 (2007).

<sup>5</sup>F. Jelezko, T. Gaebel, I. Popa, A. Gruber, and J. Wrachtrup, *Phys. Rev. Lett.* **92**, 076401 (2004).

<sup>6</sup>P. S. Fodor and J. Levy, *J. Phys.: Condens. Matter* **18**, S745 (2006).

<sup>7</sup>A. M. Tyryshkin, S. Tojo, J. J. L. Morton, H. Riemann, N. V. Abrosimov, P. Becker, H.-J. Pohl, T. Schenkel, M. L. W. Thewalt, K. M. Itoh, and S. A. Lyon, *Nat. Mater.* **11**, 143 (2012).

<sup>8</sup>M. I. Dyakonov and V. I. Perel, *Sov. Phys. JETP* **33**, 1053 (1971); *Sov. Phys. Solid State* **13**, 3023 (1972).

<sup>9</sup>J. L. Cheng, M. W. Wu, and J. Fabian, *Phys. Rev. Lett.* **104**, 016601 (2010).

<sup>10</sup>P. Li and H. Dery, *Phys. Rev. Lett.* **107**, 107203 (2011).

<sup>11</sup>H. Dery, Y. Song, P. Li, and I. Žutić, *Appl. Phys. Lett.* **99**, 082502 (2011).

<sup>12</sup>J.-M. Tang, B. T. Collins, and M. E. Flatté, *Phys. Rev. B* **85**, 045202 (2012).

<sup>13</sup>Y. Song and H. Dery, *Phys. Rev. B* **86**, 085201 (2012).

<sup>14</sup>I. Appelbaum, B. Q. Huang, and D. J. Monsma, *Nature (London)* **447**, 295 (2007).

<sup>15</sup>B. T. Jonker, G. Kioseoglou, A. T. Hanbicki, C. H. Li, and P. E. Thompson, *Nat. Phys.* **3**, 542 (2007).

<sup>16</sup>S. P. Dash, S. Sharma, R. S. Patel, M. P. de Jong, and R. Jansen, *Nature (London)* **462**, 491 (2009).

<sup>17</sup>T. Suzuki, T. Sasaki, T. Oikawa, M. Shiraishi, Y. Suzuki, and K. Noguchi, *Appl. Phys. Express* **4**, 023003 (2011).

<sup>18</sup>Y. Ando, Y. Maeda, K. Kasahara, S. Yamada, K. Masaki, Y. Hoshi, K. Sawano, K. Izunome, A. Sakai, M. Miyao, and K. Hamaya, *Appl. Phys. Lett.* **99**, 132511 (2011).

<sup>19</sup>Y. Zhou, W. Han, L.-T. Chang, F. Xiu, M. Wang, M. Oehme, I. A. Fischer, J. Schulze, R. K. Kawakami, and K. L. Wang, *Phys. Rev. B* **84**, 125323 (2011).

<sup>20</sup>A. Jain, L. Louahadj, J. Peiro, J. C. Le Breton, C. Vergnaud, A. Barski, C. Beigné, L. Notin, A. Marty, V. Baltz, S. Auffret, E. Augendre, H. Jaffrès, J. M. George, and M. Jamet, *Appl. Phys. Lett.* **99**, 162102 (2011).

<sup>21</sup>H. Saito, S. Watanabe, Y. Mineno, S. Sharma, R. Jansen, S. Yuasa, and K. Ando, *Solid State Commun.* **151**, 1159 (2011).

<sup>22</sup>K.-R. Jeon, B.-C. Min, Y.-H. Park, H.-S. Lee, C.-Y. Park, Y.-H. Jo, and S.-C. Shin, *Appl. Phys. Lett.* **99**, 162106 (2011).

<sup>23</sup>K.-R. Jeon, B.-C. Min, Y.-H. Jo, H.-S. Lee, I.-J. Shin, C.-Y. Park, S.-Y. Park, and S.-C. Shin, *Phys. Rev. B* **84**, 165315 (2011).

<sup>24</sup>A. T. Hanbicki, S.-F. Cheng, R. Goswami, O. M. J. van't Erve, B. T. Jonker, *Solid State Commun.* **152**, 244 (2011).

<sup>25</sup>K. Kasahara, Y. Baba, K. Yamane, Y. Ando, S. Yamada, Y. Hoshi, K. Sawano, M. Miyao, and K. Hamaya, *J. Appl. Phys.* **111**, 07C503 (2012).

<sup>26</sup>S. Iba, H. Saito, A. Spiesser, S. Watanabe, R. Jansen, S. Yuasa, and K. Ando, *Appl. Phys. Express* **5**, 023003 (2012); **5**, 053004 (2012).

<sup>27</sup>C. Shen, T. Trypiniotis, K. Y. Lee, S. N. Holmes, R. Mansell, M. Husain, V. Shah, X. V. Li, H. Kurebayashi, I. Farrer, C. H. de Groot, D. R. Leadley, G. Bell, E. H. C. Parker, T. Whall, D. A. Ritchie, and C. H. W. Barnes, *Appl. Phys. Lett.* **97**, 162104 (2010).

<sup>28</sup>E.-S. Liu, J. Nah, K. M. Varahramyan, and E. Tutuc, *Nano Lett.* **10**, 3297 (2010).

<sup>29</sup>E. J. Loren, B. A. Ruzicka, L. K. Werake, H. Zhao, H. M. van Driel, and A. L. Smirl, *Appl. Phys. Lett.* **95**, 092107 (2009).

<sup>30</sup>J. Rioux and J. E. Sipe, *Phys. Rev. B* **81**, 155215 (2010).

- <sup>31</sup>F. Bottegoni, G. Isella, S. Cecchi, and F. Ciccacci, *Appl. Phys. Lett.* **98**, 242107 (2011).
- <sup>32</sup>C. Guite and V. Venkataraman, *Phys. Rev. Lett.* **107**, 166603 (2011).
- <sup>33</sup>C. Hautmann, B. Surrer, and M. Betz, *Phys. Rev. B* **83**, 161203(R) (2011).
- <sup>34</sup>E. J. Loren, J. Rioux, C. Lange, J. E. Sipe, H. M. van Driel, and A. L. Smirl, *Phys. Rev. B* **84**, 214307 (2011).
- <sup>35</sup>F. Pezzoli, F. Bottegoni, D. Trivedi, F. Ciccacci, A. Giorgioni, P. Li, S. Cecchi, E. Grilli, Y. Song, M. Guzzi, H. Dery, and G. Isella, *Phys. Rev. Lett.* **108**, 156603 (2012).
- <sup>36</sup>H. Hasegawa, *Phys. Rev.* **118**, 1523 (1960).
- <sup>37</sup>L. Roth, *Phys. Rev.* **118**, 1534 (1960).
- <sup>38</sup>G. Feher, D. K. Wilson, and E. Gere, *Phys. Rev. Lett.* **3**, 25 (1959).
- <sup>39</sup>D. K. Wilson, *Phys. Rev.* **134**, A265 (1964).
- <sup>40</sup>E. M. Gershenson, N. M. Pevin, and M. S. Fogelson, *Phys. Status Solidi* **38**, 865 (1970); **49**, 411 (1972); **49**, 287 (1972).
- <sup>41</sup>R. J. Elliott, *Phys. Rev.* **96**, 266 (1954).
- <sup>42</sup>Y. Yafet, in *Solid State Physics*, edited by F. Seitz and D. Turnbull (Academic, New York, 1963), Vol. 14, p. 1.
- <sup>43</sup>V. P. Kalashnikov, *Sov. Phys. Solid State* **8**, 1693 (1967).
- <sup>44</sup>J.-N. Chazalviel, *J. Phys. Chem. Solids* **36**, 387 (1975).
- <sup>45</sup>D. Gershoni, C. H. Henry, and G. A. Baraff, *IEEE J. Quantum Electron.* **29**, 2433 (1993).
- <sup>46</sup>G. L. Bir and G. E. Pikus, *Symmetry and Strain-Induced Effects in Semiconductors* (Halsted, Jerusalem, 1974), Chaps. 3 and 4.
- <sup>47</sup>E. L. Ivchenko and G. E. Pikus, *Superlattices and Other Heterostructures* (Springer, Heidelberg, 1995).
- <sup>48</sup>R. Winkler, *Spin-Orbit Coupling Effects in Two-Dimensional Electron and Hole Systems* (Springer, Berlin, 2003), Appendix B.
- <sup>49</sup>R. Winkler and U. Zülicke, *Phys. Rev. B* **82**, 245313 (2010).
- <sup>50</sup>C. Kittel, *Quantum Theory of Solids* (Wiley, New York, 1963).
- <sup>51</sup>A. A. Maradudin, E. W. Montroll, G. H. Weiss, and I. P. Ipatova, in *Solid State Physics*, 2nd ed., edited by H. Ehrenreich, F. Seitz and D. Turnbull (Academic, New York, 1963), Suppl. 3.
- <sup>52</sup>All these Hamiltonian terms form invariants under all crystal symmetry operations. So they belong to IRs of  $\Gamma$ -point group and thus are IRs of its subgroup at  $\mathbf{K}_0$  or wave vector connecting two points of  $\mathbf{K}_0$  star.
- <sup>53</sup>W. Weber, *Phys. Rev. B* **15**, 4789 (1977).
- <sup>54</sup>G. Nilsson and G. Nelin, *Phys. Rev. B* **6**, 3777 (1972).
- <sup>55</sup>M. Lax and J. J. Hopfield, *Phys. Rev.* **124**, 115 (1961).
- <sup>56</sup>H. W. Streitwolf, *Phys. Status Solidi* **37**, K47 (1970).
- <sup>57</sup>G. Dresselhaus, A. F. Kip, and C. Kittel, *Phys. Rev.* **98**, 368 (1955).
- <sup>58</sup>J. Li, L. Qing, H. Dery, and I. Appelbaum, *Phys. Rev. Lett.* **108**, 157201 (2012).
- <sup>59</sup>J. R. Chelikowsky and M. L. Cohen, *Phys. Rev. B* **14**, 556 (1976).
- <sup>60</sup>P. Y. Yu and M. Cardona, *Fundamentals of Semiconductors*, 3rd ed. (Springer, Berlin, 2005), Chap. 2.
- <sup>61</sup>M. S. Dresselhaus, G. Dresselhaus, and A. Jorio, *Group Theory, Application to the Physics of Condensed Matter* (Springer, Berlin, 2010), Chap. 12.
- <sup>62</sup>Terms that scale with  $\gamma_j^2 O(k^2)$  were omitted since  $\gamma_j \ll 1$ .
- <sup>63</sup>In Si, scattering with long-wavelength optical and acoustic phonons becomes comparable at room temperature (when the population of optical phonons is no longer negligible). The reason for the negligible contribution of optical modes to intravalley spin relaxation in Ge stems from the different symmetries of the electronic wave functions at the vicinity of the  $L$  point (Ge) and the  $\Delta$  axis (Si).
- <sup>64</sup>Scattering symmetries that are inherent to the electronic states are kept. However, approximating the electron-phonon interaction by  $\Xi q$  masks other scattering symmetries along certain high-symmetry directions. Replacing the scalar interaction with the correct tensorial form restores these scattering symmetries (see Ref. 13 for further details).
- <sup>65</sup>B. Huang, D. J. Monsma, and I. Appelbaum, *Phys. Rev. Lett.* **99**, 177209 (2007).
- <sup>66</sup>E. O. Kane, *J. Phys. Chem. Solids* **1**, 249 (1957).
- <sup>67</sup>H. Dery, Ł. Cywiński and L. J. Sham, *Phys. Rev. B* **73**, 161307(R) (2006).
- <sup>68</sup>Ł. Cywiński, H. Dery and L. J. Sham, *Appl. Phys. Lett.* **89**, 042105 (2006).
- <sup>69</sup>J. Fabian, A. Mathos-Abiague, C. Ertler, P. Stano, and I. Žutić, *Acta Phys. Slov.* **57**, 565 (2007).
- <sup>70</sup>R. de Sousa, C.-C. Lo, and J. Bokor, *Phys. Rev. B* **80**, 045320 (2009).
- <sup>71</sup>F. Herman and S. Skillman, *Atomic Structure Calculations* (Prentice-Hall, Englewood Cliffs, NJ, 1963).
- <sup>72</sup>M. M. Rieger and P. Vogl, *Phys. Rev. B* **48**, 14276 (1993).
- <sup>73</sup>O. H. Nielsen and W. Weber, *Comput. Phys. Commun.* **18**, 101 (1979).
- <sup>74</sup>J. Tauc and E. Antončík, *Phys. Rev. Lett.* **5**, 253 (1960).